CHAPTER 5

In this chapter, the results obtained from P and S receiver function analysis are presented and discussed. The receiver functions have been derived using the three-component seismological data in the study area in order to delineate the crustal and upper mantle structures beneath Greece and Aegean Sea.

5. Results and Discussions

Since two different methods used in this thesis, the results were also divided into two parts. Firstly, the crustal and upper mantle structures are deduced from P receiver function method and in the second part, results obtained from S receiver function method are shown and discussed. The results are interpreted in a unified way and compared with previous works.

5.1 Results from P receiver functions

5.1.1 Observed P receiver functions

Teleseismic P receiver functions were computed by using theoretical back azimuth and incidence angle as explained in chapter 3 for each station. A distance (moveout correction) correction was applied prior to stacking to achieve high signal to noise ratio. Figures 5.1-5.3 show P receiver functions for six stations located in different parts of the study area.

Distance-corrected receiver functions using a reference distance of 67° for station LIMN, LESB located in northern Aegean Sea and ALEX and NEO located in mainland Greece are shown in Figure 5.1-5.2. The P receiver functions were sorted according to their increasing back azimuth. Red cubes indicating back azimuth, while epicentral distances are plotted with black circles. The data have been filtered between 1 and 10 s and are plotted in a time window of -5 to 20 s in order to give information for both continental and oceanic lithospheric structures.

Positive amplitudes are shaded in black and indicate (if caused by direct conversion) an increasing velocity with depth, whereas negative amplitudes (shaded in gray) demonstrate velocity decreasing downwards. The P onset is fixed to be as zero time. The sum traces in the upper panels present the stacked P receiver function for each station. At stations shown in Figure 5.1-5.2, P receiver functions exhibit clear primary Ps conversion from the Moho and multiply-reflected phases, which reverberate between earth's surface and Moho discontinuity. The Ps conversions from the Moho arrive at delay time of about 3-4 s, while the multiples are observed at 10-14 s delay time. However, the arrivals of the multiple phases are not clear shown in receiver functions. Another Ps conversion observed at about 0.5 s is attributed to the sedimentary layer, which is significantly located below the surface. P receiver functions for two other stations KARP and ZKR located at the forearc of the subduction; in the southern Aegean Sea and on the island of Crete, respectively, show another feature (Fig. 5.3). Asides from the clear Ps conversion from a sedimentary layer, which can be observed at about 1 s, a very stable and dominant converted phase can be also identified at about 6 s delay time. This phase is clearly related to the oceanic Moho of the subducting African plate, which can be clearly observed beneath forearc area of the subduction. The absence of the converted Moho phase (Fig. 5.3) with positive amplitude is however clearly demonstrated by receiver functions.

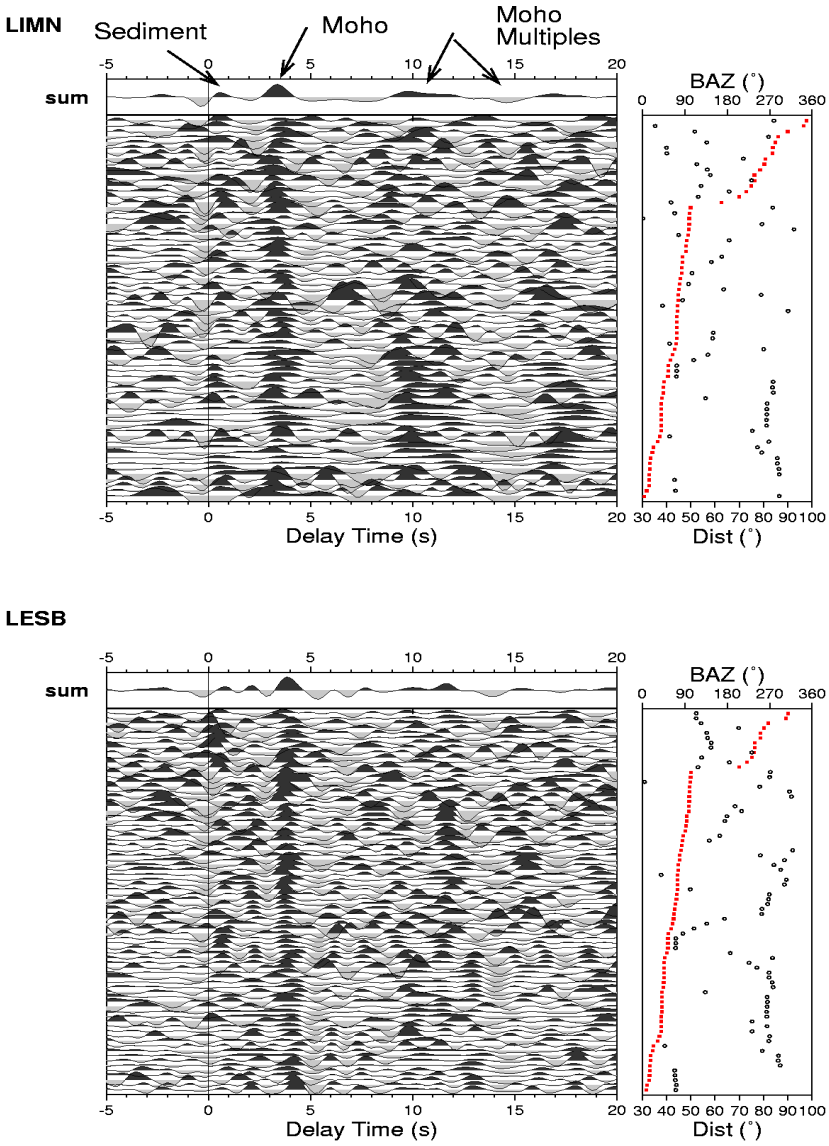

Fig. 5.1. Individual P receiver functions for the two stations LIMN and LESB located in northern Aegean Sea. The moveout-corrected receiver functions are sorted by their back azimuth and filtered with bandpass filter 1-10 s. Red cubes show back azimuth and epicentral distances are indicating by black circles. The summation traces at the top of the figures represent clearly the Ps converted phases from sediment at ~ 0.5 s, whereas Ps conversions from Moho arrives at 3-4 s delay time. The Moho multiples are not well identified in the data, but arrive near 10-14 s delay time.

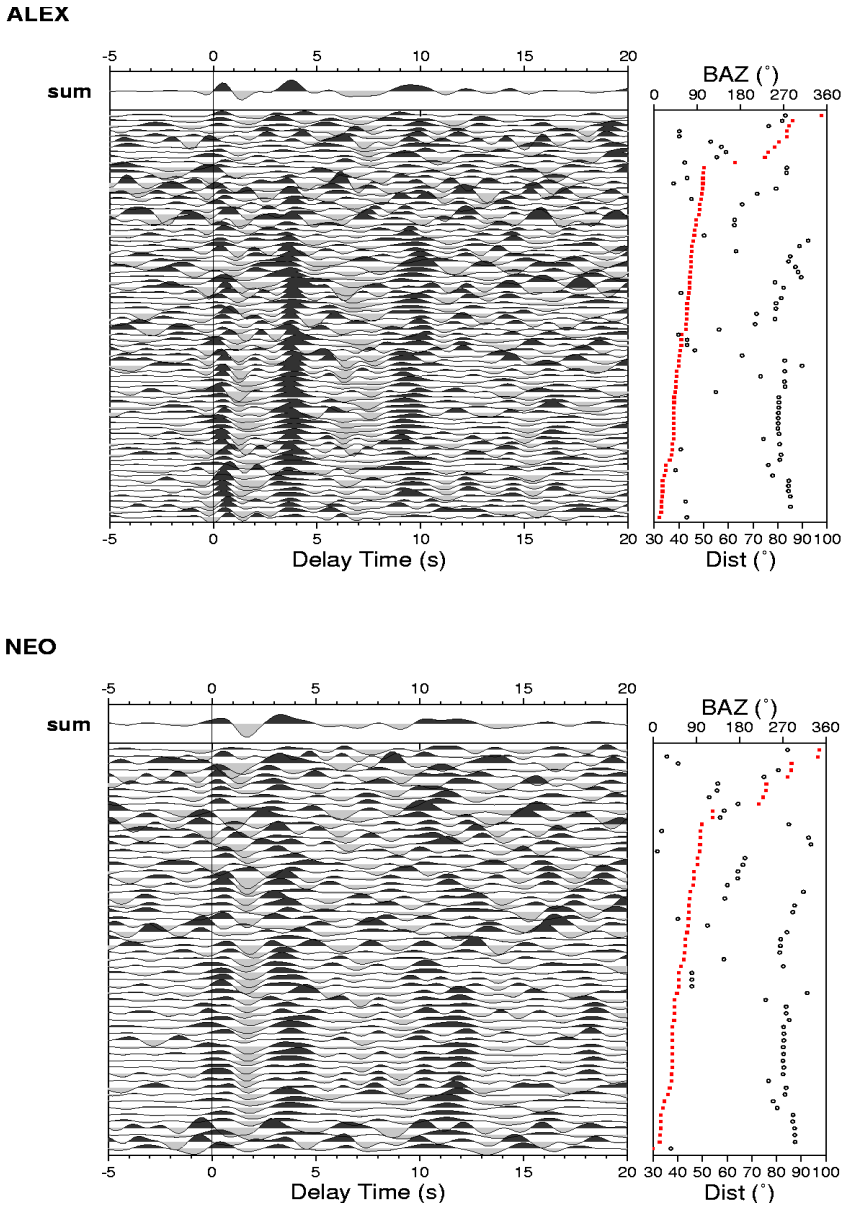

Fig. 5.2. Individual P receiver functions for the two stations ALEX and NEO located in mainland Greece. The arrival times of the Ps converted phase from sediment and Moho boundary as well as Moho multiples can be clearly seen in the summation traces shown at the top of the figures.

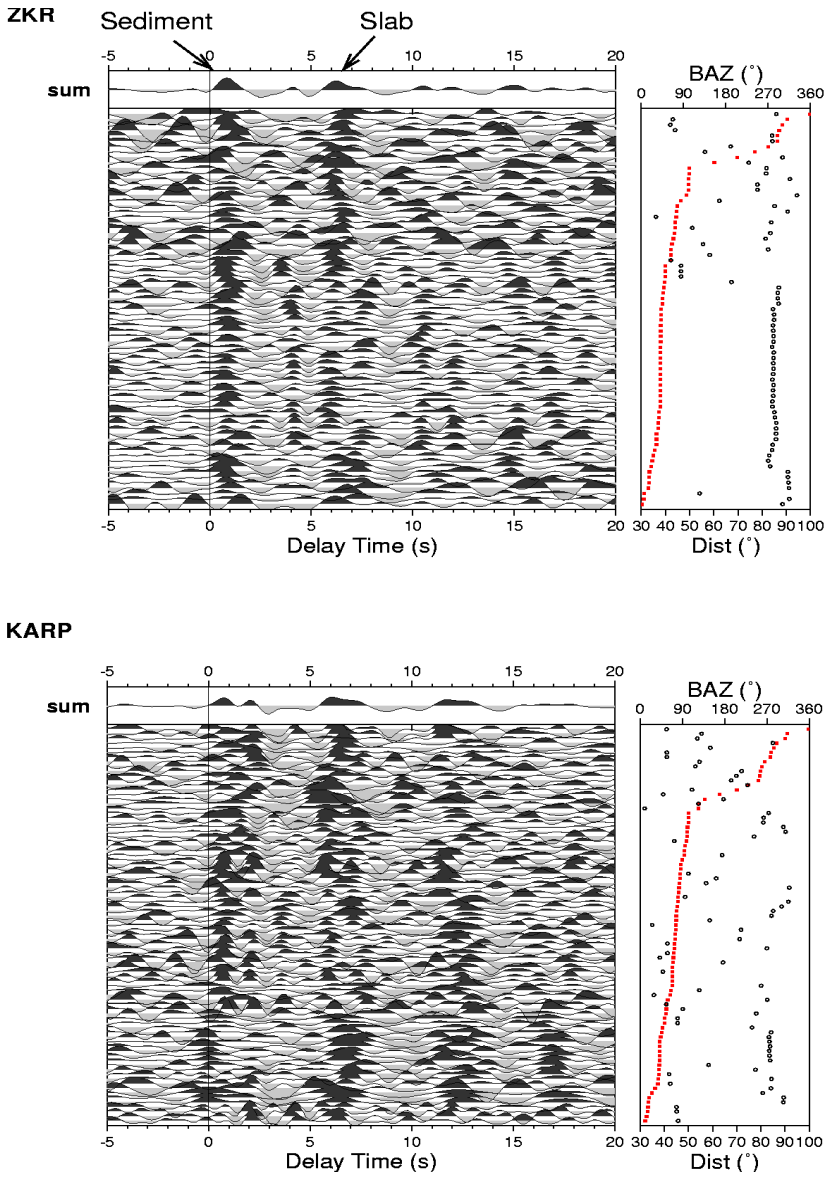

Fig. 5.3. Moveout-corrected P receiver functions obtained from the two stations ZKR and KARP located at the forearc area of the subduction show no clear conversion from the Moho boundary, while the arrival times of the Ps conversion from sediment and African Moho (slab) are well imaged.

This phase can not be identified for these two stations, while it was well observed at the other stations located in northern Aegean Sea and continental Greece.

5.1.2 Reversed Moho contrast in the forearc

To have a glimps of the crustal structure in the entire area, the results from P receiver functions for all stations are summarized in Fig. 5.4. The stacked P receiver functions obtained from each station are sorted by their relative distance to the Hellenic trench, from south to north, and provide an average thickness beneath each station. They were filtered between 1-20 s. The number of receiver functions stacked is also indicated with the station code in parenthesis. The observed energy at time 0 for some stations suggests that either the rotation of the components is not optimal or that local sediments generate some energy.

Regarding Figure 5.4, the receiver functions obtained for stations in the southern Aegean and on the island of Crete (labeled with FA in Figure 5.4) reveal clearly an increase of Ps delay time toward the north, reaching a 10 s delay time beneath the volcanic arc. This phase is related to the oceanic Moho of the subducted African plate, which will be referred to as “slab” hereinafter. This phase can be followed from 4.5 s beneath station VLS in western Peleponnesus to 11 s beneath station SANT at the volcanic arc (labeled with VA). However, further north, the identification of this phase is not clear anymore. Under the stations located in the northern Aegean Sea and in continental Greece (labeled with NA and CG, respectively), the converted Ps energy is clearly observed between 3 and 4.8 s. This phase is related to the Moho of the continental Aegean plate, which will be referred to as “Moho” hereinafter. This phase is however not well observed under the southern part of the region (FA). Of interest, a significant converted phase with a negative amplitude is observed at some stations located in the forearc (marked with a dashed red box). This negative phase observed for the most stations at Crete, (Knapmeyer, 2000; Li et al., 2003; Endrun et al., 2004) has also been reported in the Cascadia subduction zone (Bostock et al., 2001) and was interpreted to be due to a reversed Moho velocity contrast caused by the hydration and serpentinization of mantle minerals in the forearc.

Since serpentinite has shear wave velocity lower than the crustal velocities, it causes a reversed Moho contrast in the mantle wedge. However, this phase can not be followed beneath stations located in northern Aegean Sea and continental Greece.

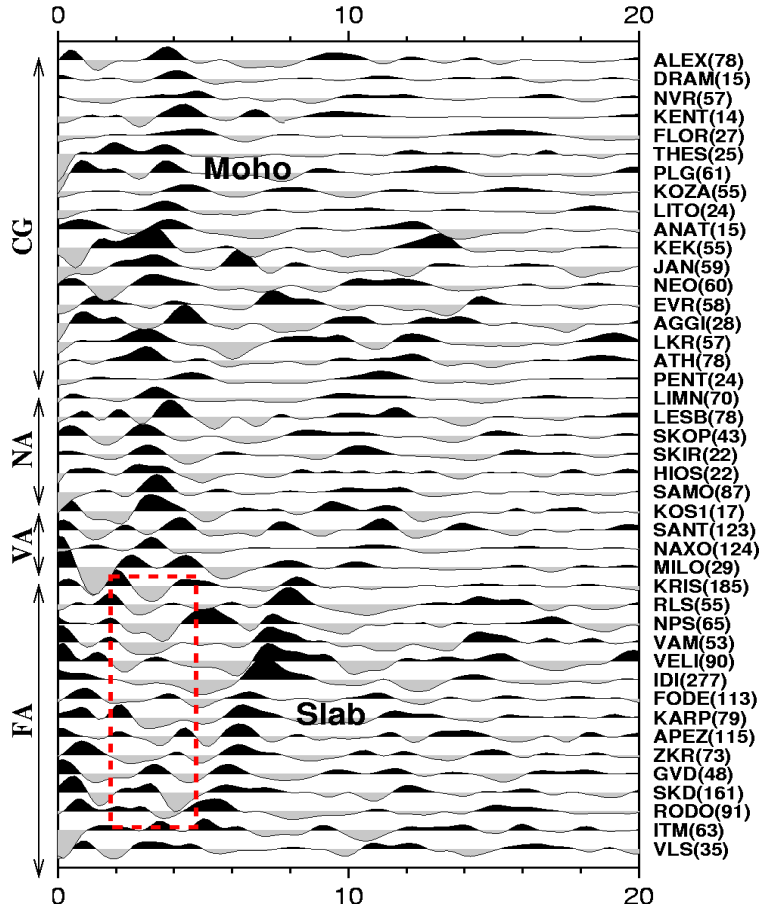

Fig. 5.4. Stacked P receiver functions sorted according to their distance from the Hellenic trench from forearc to mainland Greece. The north dipping phase in the southern part labeled "Slab" indicates Ps conversions from the Moho of the subducting oceanic African plate. This phase can be traced from station VLS in western Peleponnesus to the station SANT at the volcanic arc (or may continue till 13 s) . Ps conversions from the Moho of the continental Aegean plate are observed in the northern part beneath NA and CG and disappears southward. Red dashed line underlines clear negative conversions observed beneath FA at the expected Moho times. The number of P receiver functions for each station is also shown in brackets. FA = forearc, VA = volcanic arc, NA = northern Aegean and CG = continental Greece.

5.1.3 Calculating Moho depth from Ps conversions

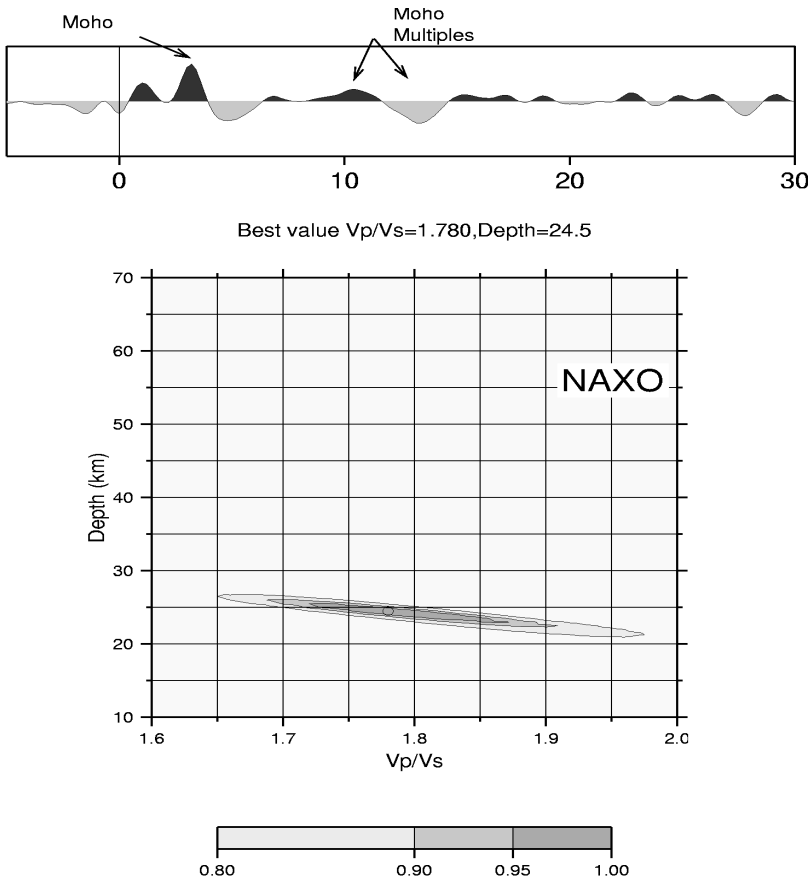

Fig. 5.5. Successful application of Zhu and Kanamori method for station NAXO with relatively clear multiple phases shows a Moho depth of 24.5 km and average Vp/Vs ratio of 1.78.

To compute the Moho depth, the Zhu and Kanamori method could not successfully be utilized for all stations. Since this method looks for the primary conversion of the Moho as well as multiples , in absence of clear multiples, the computed Moho depth and Vp/Vs ratio will be unrealistic. However, in presence of good multiple phases the crustal parameters have been derived in some cases. Figure 5.5 shows an example of successful application of Zhu and Kanamori method for station NAXO located in the Cyclades where the clear multiples are observed. The Moho depth and Vp/Vs ratio are

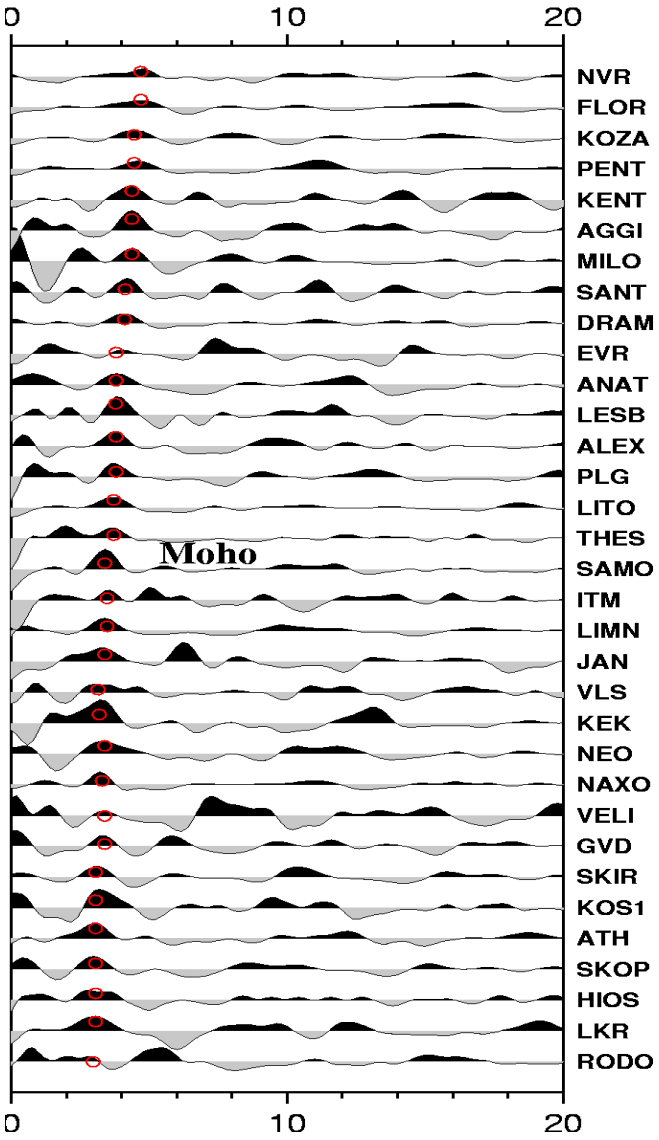

Fig. 5.6. The stacked P receiver functions for stations with observed normal Moho contrast are sorted according to the increasing time of their Moho conversions. No clear multiples can be seen in the data. Moho arrival times are converted into depth values using Vp of 6.2 km/s and Vp/Vs ratio of 1.73.

computed using the arrival times of Ps converted phases from the Moho as well as its multiples, which are marked on the stacked receiver functions. But to construct a homogeneous Moho map for the whole area, a unique method is needed, which could

be similarly performed for all stations without considering the multiples. In Figure 5.6, the stacked P receiver functions are sorted by increasing time of the converted Ps Moho phase. The data show clear primary Moho conversions with arrival times ranging between 3-4.8 s, even though Moho multiples are not significantly visible in the data. To compute the Moho depth for the stations with observed positive Moho phase, a reference crustal velocity of 6.2 km/s and Vp/Vs ratio of 1.73 (similar to the IASP91 reference model) were used. The calculated Moho depths are shown in Table C.1, Appendix C. No estimation of the delay times of Moho converted phase obtained from stations in the forearc was attempted, due to their negative amplitudes.

5.1.4 Calculated Slab depth from Ps conversions

The delay times of the observed slab phase are also converted into depth, using the IASP91 reference model. The delay time of the slab phase is estimated from the P receiver functions if it is clearly visible in the data. The delay times of the slab phase and corresponding depth values are listed in Table C.1, Appendix C.

5.1.5 Receiver function migration

To generate a depth section, the receiver functions for each station are migrated in space and projected onto three vertical profiles (Fig. 5.7) trending normal to the Hellenic trench in the western, central and eastern part of the Hellenic arc. Also included in Figure 5.7 is the epicenters of shallow and intermediate depth earthquakes occuring in this region (mb >= 4.5) along the Hellenic arc (Engdahl et al., 1998). As the seismicity shows, the deep earthquakes (~ 180 km) are located in the southeastern part of the Aegean beneath the Dodecanese islands.

The obtained 2D migrated sections along three profiles are represented in Fig. 5.8. Positive amplitudes of receiver functions are plotted in red, while negative amplitudes are in blue.

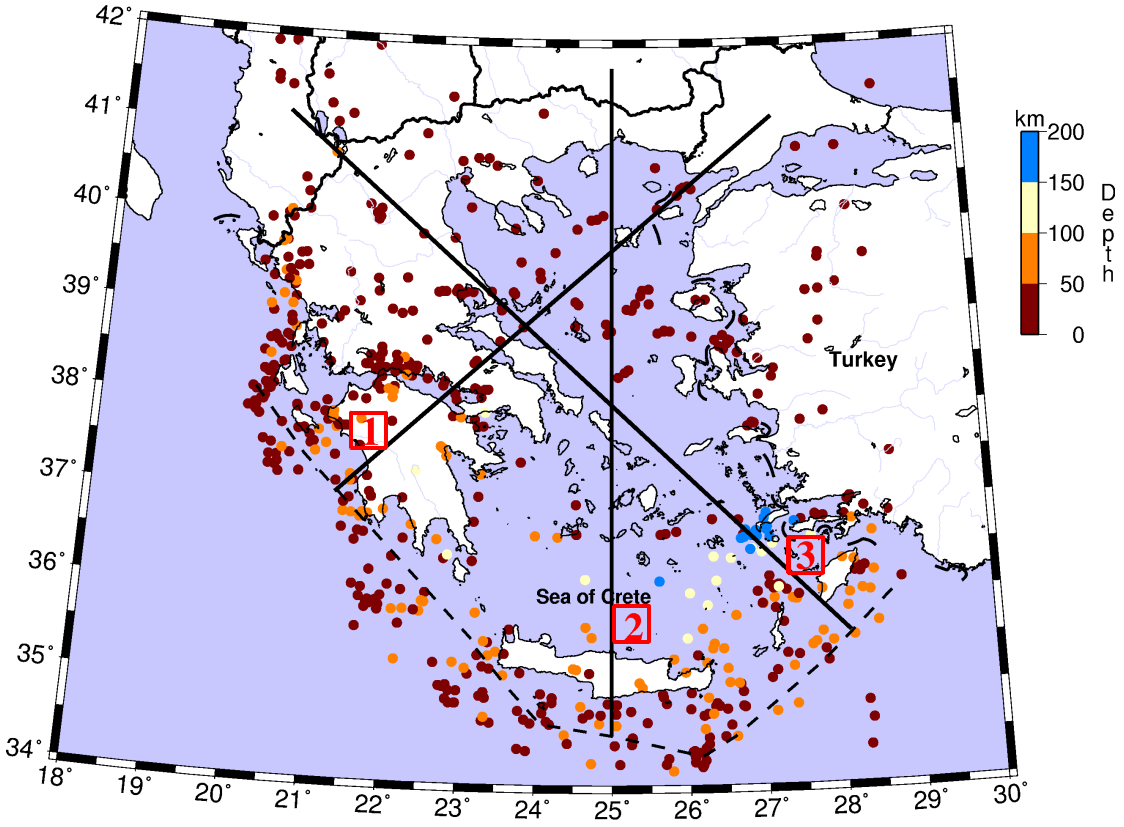

Fig. 5.7. Epicenters of the shallow and intermediate depth earthquakes (mb >= 4.5) across the whole Aegean shows that the deepest earthquakes are located in the southeastern part of the Aegean beneath Dodecanese islands (~ 180 km). Three vertical profiles normal to the Hellenic trench are considered to image the Hellenic slab beneath each part of the area.

The seismicity along the profile is also plotted on each section as an evidence for the presence of the subducted slab. The subducted African slab can not be well identified by these cross-sections, however, the seismicity reliably shows an increasing in the slope of the downgoing slab towards east.

A 2D migrated receiver function section obtained from the summation of all three profiles, displays an average image of the continental Moho and of the descending slab (Fig. 5.9). The seismicity could not be plotted on this migrated section, due to the summation of three different profiles with varying geometry for the subducted oceanic plate.

The converted phase associated with the continental Moho is observed under the northern Aegean Sea and mainland Greece (labeled with NA and CG, respectively) at depths ranging from 30 to 40 km, while further south this phase disappears. The subducting oceanic Moho is reliably imaged from ~ 35 to about 100 km depth in the volcanic region. However, this image can not be considered as the absolute shape of the slab because the summation is affected by data quality and the number of events, which are not the same along all the three profiles, and insufficient for a meaningful migration.

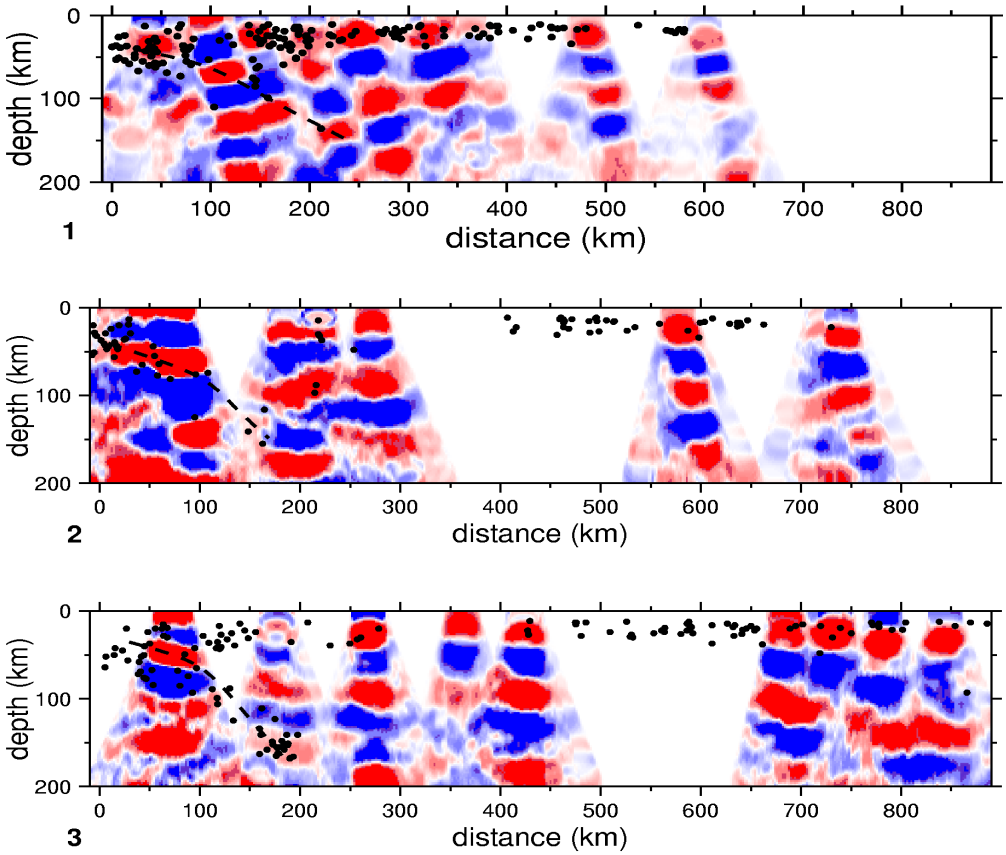

Fig. 5.8. 2D migrated P receiver function sections along three profiles located in the western, central and eastern part of the Hellenic arc shown in Figure 5.8. The positive amplitudes of receiver function are plotted in red, while blue color shows negative amplitudes. The seismicity is also projected on each cross-section. Although the descending African slab is not well resolved on the cross-sections , seismicity shows reliably an increasing in the slope of the subducted slab towards east.

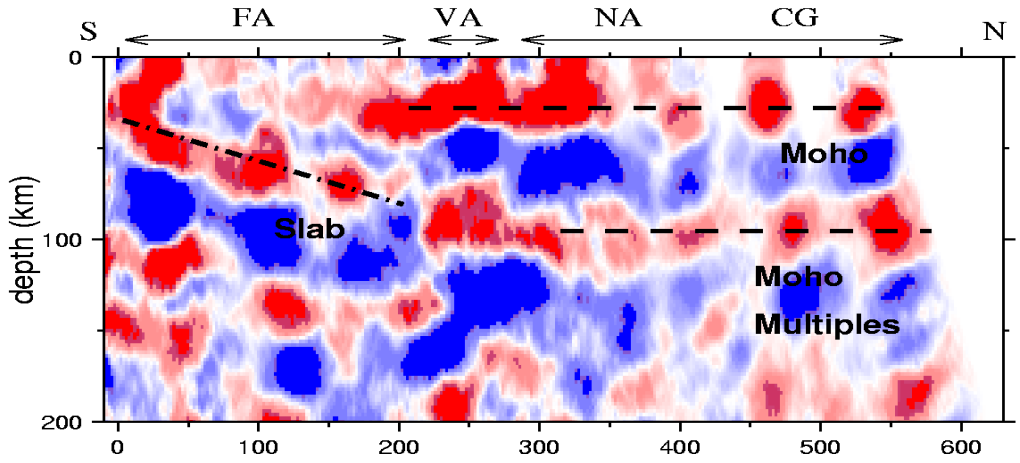

Fig. 5.9. 2D migrated P receiver function section obtained from the summation of the three profiles normal to the Hellenic trench, shown in Figure 5.8. The continental Aegean Moho and its multiples as well as the subducted oceanic African Moho are indicated by labeled dashed lines. The slab can be identified beneath forearc area and volcanic arc (shown with FA and VA), which reaches the depth of 100 km under volcanic arc. The Moho boundary beneath northern Aegean Sea and continental Greece (NA and CG) is clearly imaged at 30-40 km. The continuation of the continental Moho due to negative amplitudes in the forearc is less clear.

5.2 Results from S receiver functions

5.2.1 Observed S receiver functions

The new technique of S receiver functions (Kumar et al., 2005) has been applied to different datasets across the whole study area. The theoretical back azimuth and observed incidence angle were used to calculate the S receiver function (as shown in chapter 3). Moveout and bandpass filtered (6-20 s) S receiver functions of the GEOFON station KRIS located on the island of Crete is shown in Figure 5.10. In order to compare receiver functions obtained from both the methods, the S receiver functions are plotted in reversed time and the polarities are also reversed. The negative

amplitudes are plotted in black and indicate velocity decreasing downwards, while positive amplitudes in gray show an increasing velocity with depth. The S receiver functions are sorted by their back azimuth marked at the right.

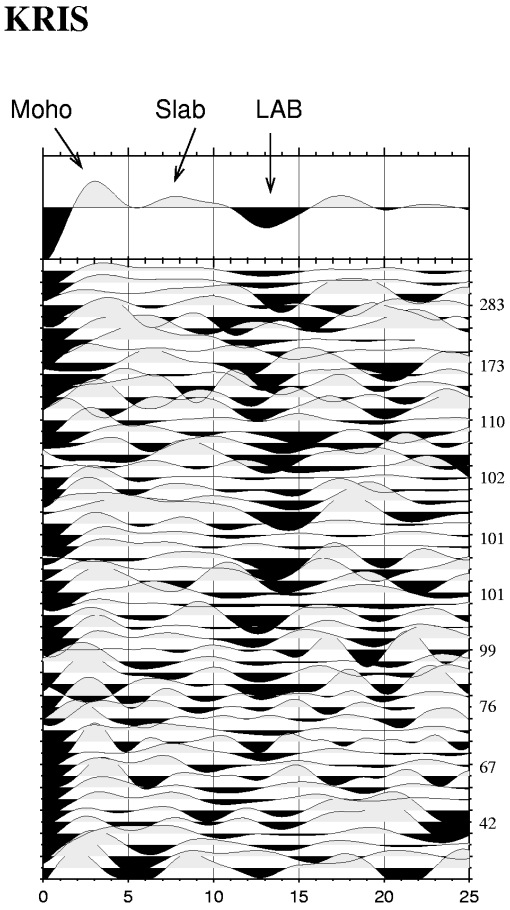

Fig. 5.10. Individual S receiver functions for station KRIS on the island of Crete are sorted by their back azimuth (shown at the right). Negative amplitudes are plotted in black and indicate velocity decreasing downwards. The S receiver functions are plotted in reverse time in order to compare with P receiver functions. The arrows on the stacked trace show the average time of the Sp conversions generated by the continental Moho, the oceanic Moho of the subducted slab and the lithosphere-asthenosphere boundary, respectively.

Three phases are visible on the records, which are marked on the summation trace at the top in Figure 5.10 . The first phase, at about 3 s, shows the converted Sp phase due to the Moho discontinuity, the second phase at about 8 s is related to the oceanic Moho of the descending slab. The third phase, which has a strong negative amplitude

(velocity decreasing downwards) at about 13 s delay time is interpreted as due to the lithosphere-asthenosphere boundary (labeled with LAB). This phase is usually not seen in P receiver functions because it is masked by crustal multiples arriving at nearly the same time.

5.2.2 Distribution of piercing points

S receiver functions are computed for all stations in a same way. Unlike P receiver functions, the Sp conversions are not located close to the stations and show additionally significant overlapping with the Sp conversions obtained from adjacent stations. In Figure 5.11 the location of the piercing points at 80 km depth (likely to be approximately the thickness of the LAB) for the Ps and Sp conversions are plotted. While P piercing points are located (laterally) close to the recording stations, S piercing points are located much farther away. The lack of P receiver function data in the Sea of Crete can be seen clearly in Figure 5.11, which makes the P receiver function map of the Moho and downgoing slab less certain under this region. However, the Sea of Crete and central Aegean are well covered with S receiver function data. Due to the wider lateral distribution of piercing points for the S receiver functions compared to those of P receiver functions as well as the overlap of S piercing points from neighbor stations, the crustal and upper mantle structure can not be studied by considering S receiver functions from individual stations.

5.2.3 Descending oceanic African Moho

To illustrate the slab geometry from S receiver functions, two sets of cross-sections are considered. The whole study area can also well be covered by selected cross-sections. The first set consists of three N-S trending cross-sections parallel to each other across the Aegean and continental Greece (Fig. 5.12). The profiles A and B are located in the eastern and middle part of the Hellenic arc, respectively, while profile C

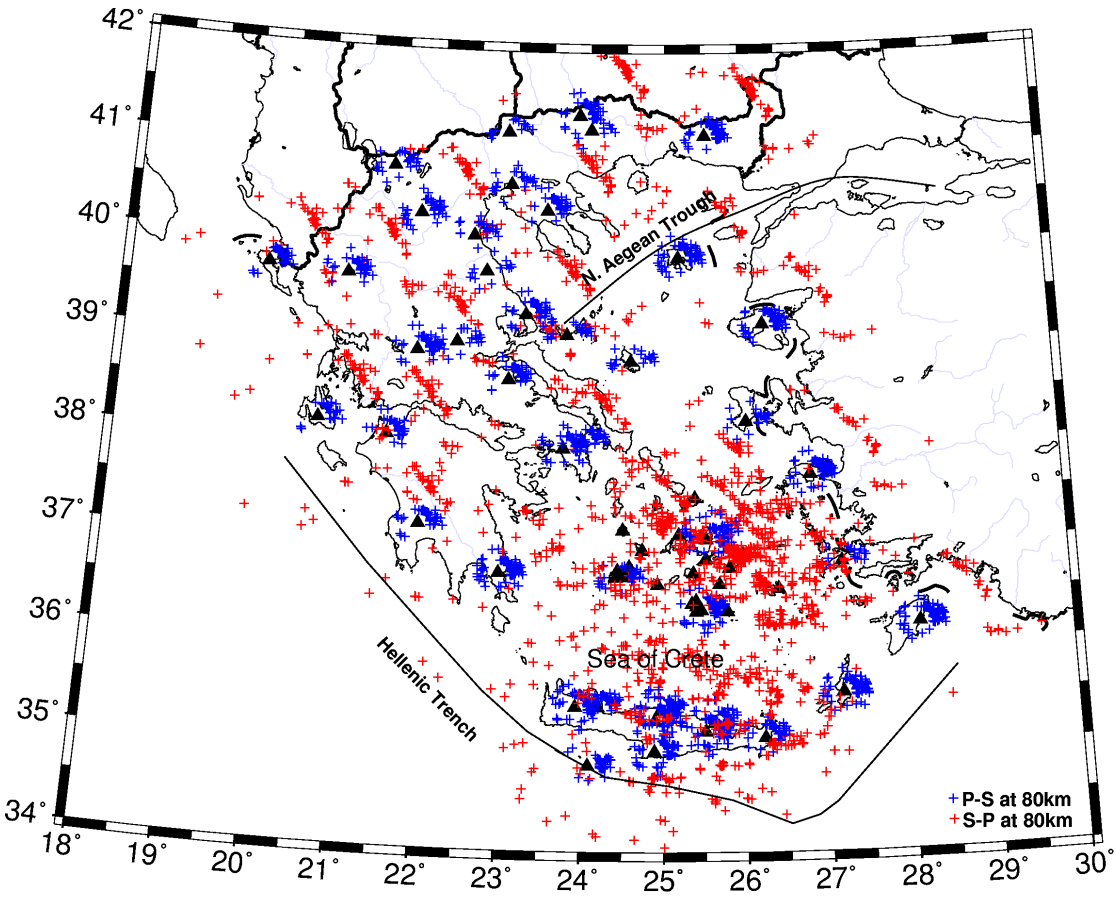

Fig. 5.11. Location of piercing points of P and S receiver functions at 80 km depth. Stations are indicated by triangles. While P piercing points are located close to the stations, the S piercing points occurred much farther away. The Sea of Crete is well covered with S piercing points.

crosses Peleponnesus and western continental Greece. The next set consists of three profiles perpendicular to the Hellenic trench, shown in Figure 5.13. The profiles D, E and F are located normal to the trench in the eastern, middle and western part of the Hellenic arc, respectively. Individual S receiver functions are sorted by the latitude of their piercing points at 80 km depth along each profile, shown in Figures 5.14 and 5.15. Positive amplitudes are plotted in black. Although the individual traces are much noisier than stacked data, they allow a more detailed image of the Moho and of the subduction.

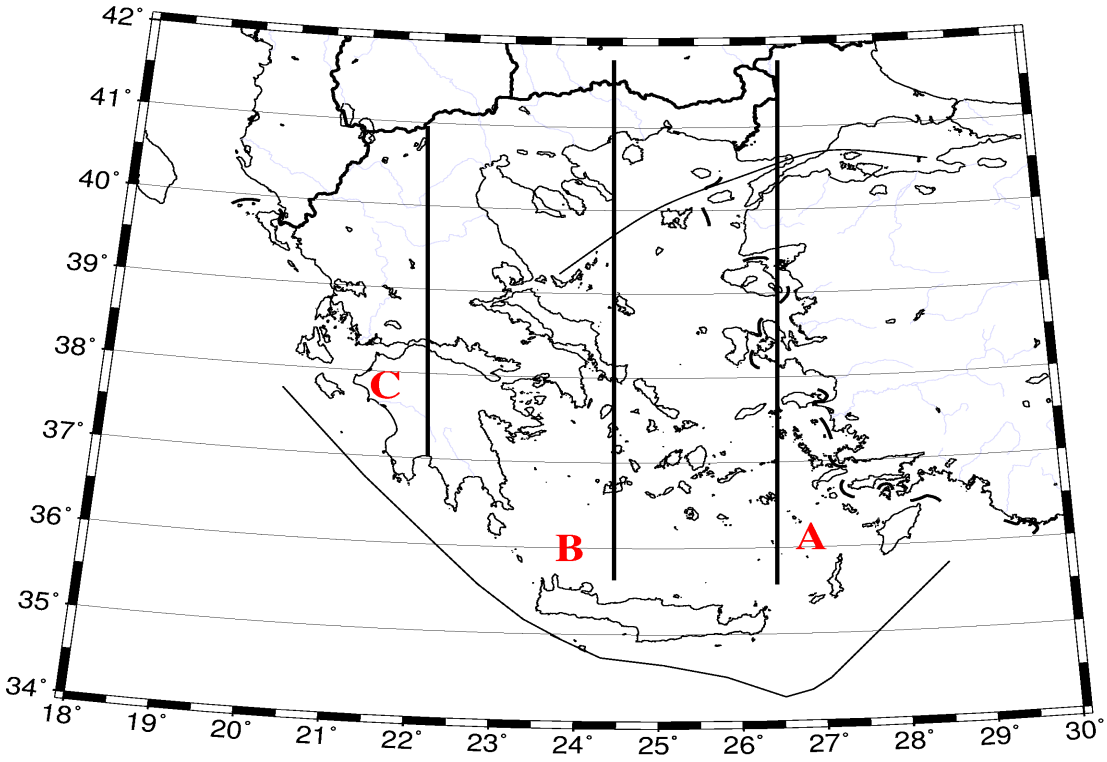

Fig. 5.12. Positions of three parallel cross-sections (A, B, C) in the eastern, central and western part of the Hellenic trench.

5.2.4 Slab geometry obtained from Profiles A-C

As Figure 5.14 shows, asides from the primary converted phase from the Moho discontinuity, which can be seen between 2.5 to 4 s along profile A, a very strong and coherent phase can be also followed from 6 s (~ 50 km deep) in the southern Aegean down gradually to about 25 s (~ 230 km deep) in the northern Greece. This dipping phase is clearly related to the oceanic Moho of the subducting African plate. Due to the lack of seismological stations in the Aegean Sea the oceanic Moho could be only imaged by P receiver functions to 10 s beneath station SANT in the volcanic arc.

Along profile A, the downgoing slab has a noticeably variable slope. It starts at low angle in the southern Aegean and becomes steeper under the volcanic arc. It flattens out beneath the central Aegean and then steepens again beneath the northern Aegean Sea and continental Greece.

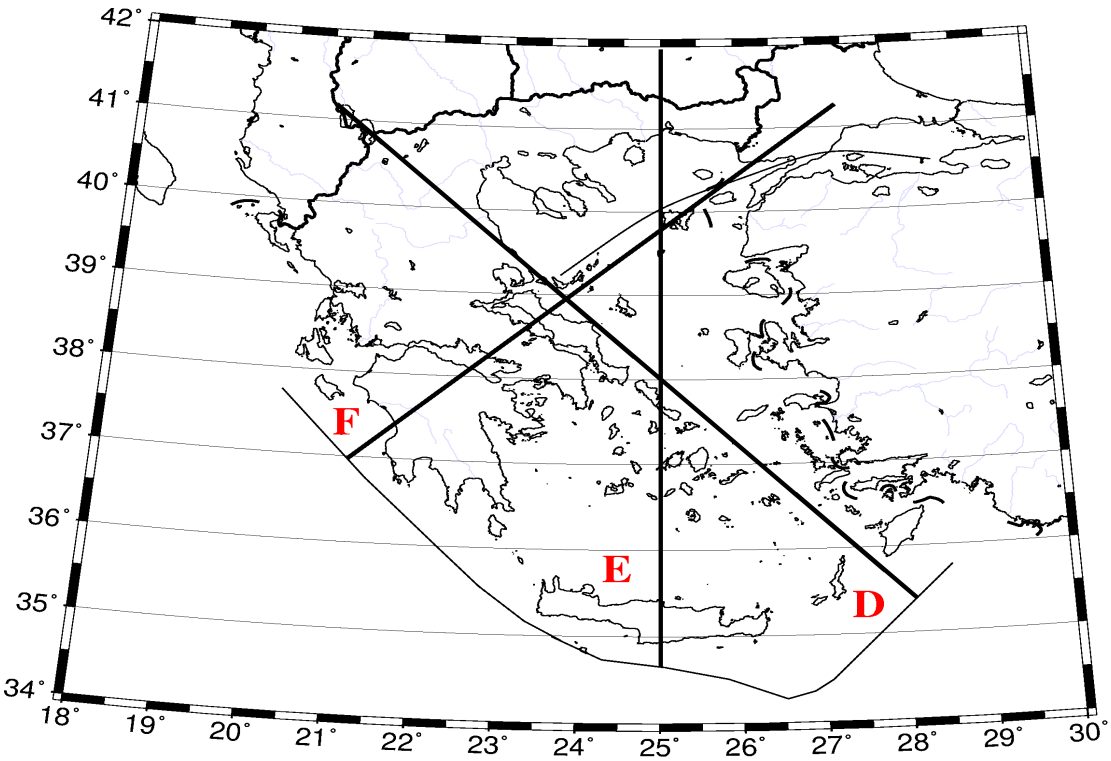

Fig. 5.13. Positions of next three profiles (D, E, F) normal to the Hellenic trench in the eastern, middle and western part of the arc.

In the central part of the Hellenic subduction zone, along profile B, the slab is clearly deeper than in the eastern part. It can be followed from 9 s in the southern Aegean down to 23 s beneath the northern Greece. It also dips gradually at a low angle to the northern Aegean and becomes horizontal towards mainland Greece. Beneath western Peleponnesus and western Greece, along profile C, the Hellenic slab is shallow and arrives at delay time of 5-6 s. The arrival of this slab converted phase is very close to that of the Moho converted phase, which seen at about 3 s. However, according to Figure 5.14 (C), there is no doubt that the converted phase at 5 s beneath Peleponnesus is associated with the Hellenic slab. The slab is almost horizontal beneath Peleponnesus, dips steeply (~ 45°) beneath the Gulf of Corinth and flattens out under continental Greece.

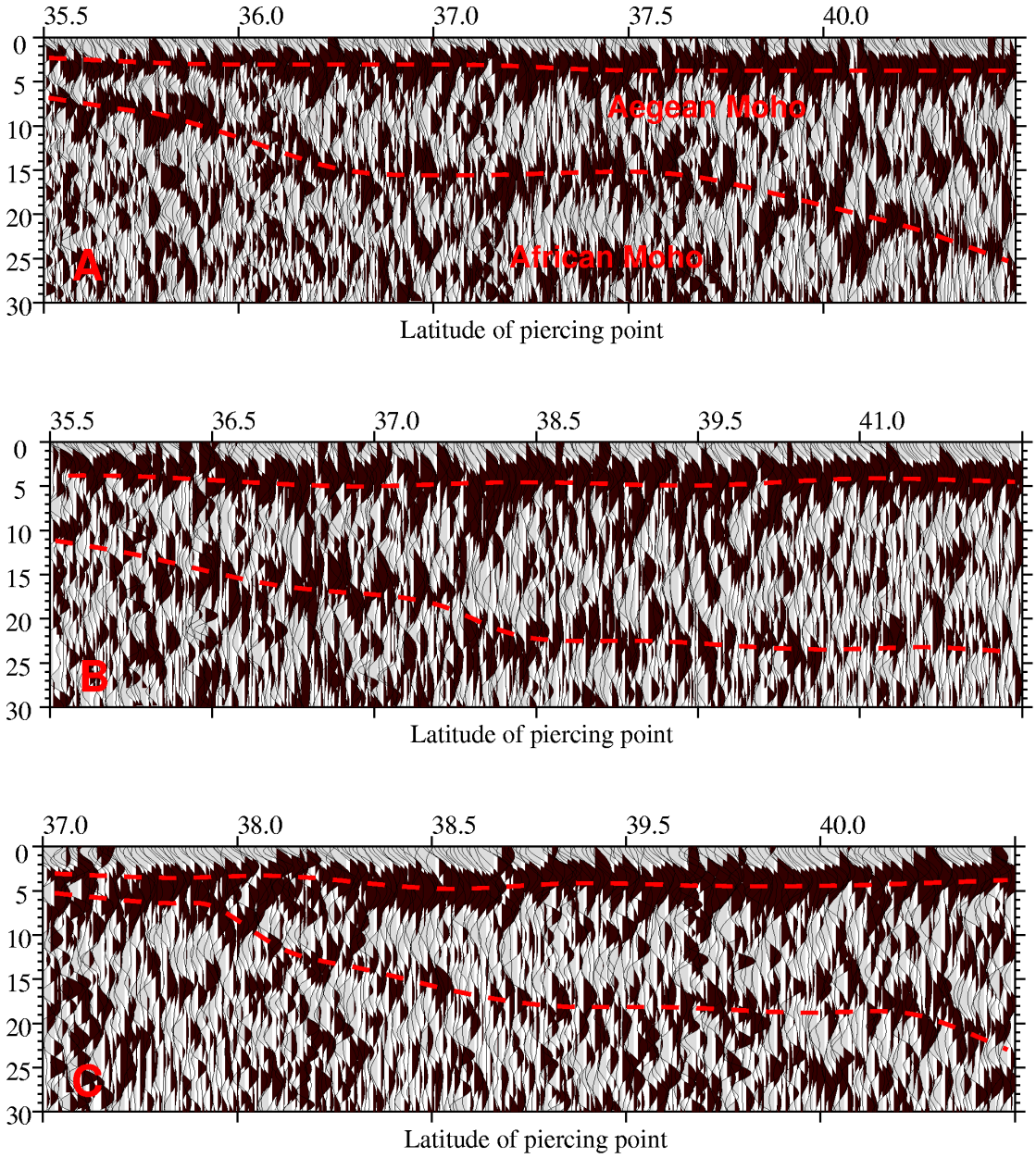

Fig. 5.14. The imaged structures deduced from individual S receiver functions along NS trending profiles A-C. The converted phases are underlined with a red dashed line. The first converted phase is related to the continental Aegean Moho and the second phase to the subducting African slab. A) individual S receiver functions sorted after latitude of S piercing points at 80 km along eastern profile A. The Moho and the downgoing slab are well demonstrated up to northern Greece. B) same for profile B in the middle part of the Hellenic arc. C) same for profile C located in the western part of the arc, which shows a shallower slab than the other parts of the arc. Towards north the slab shows a more straight form in comparison to its shallower part.

5.2.5 Slab geometry obtained from profiles D-F

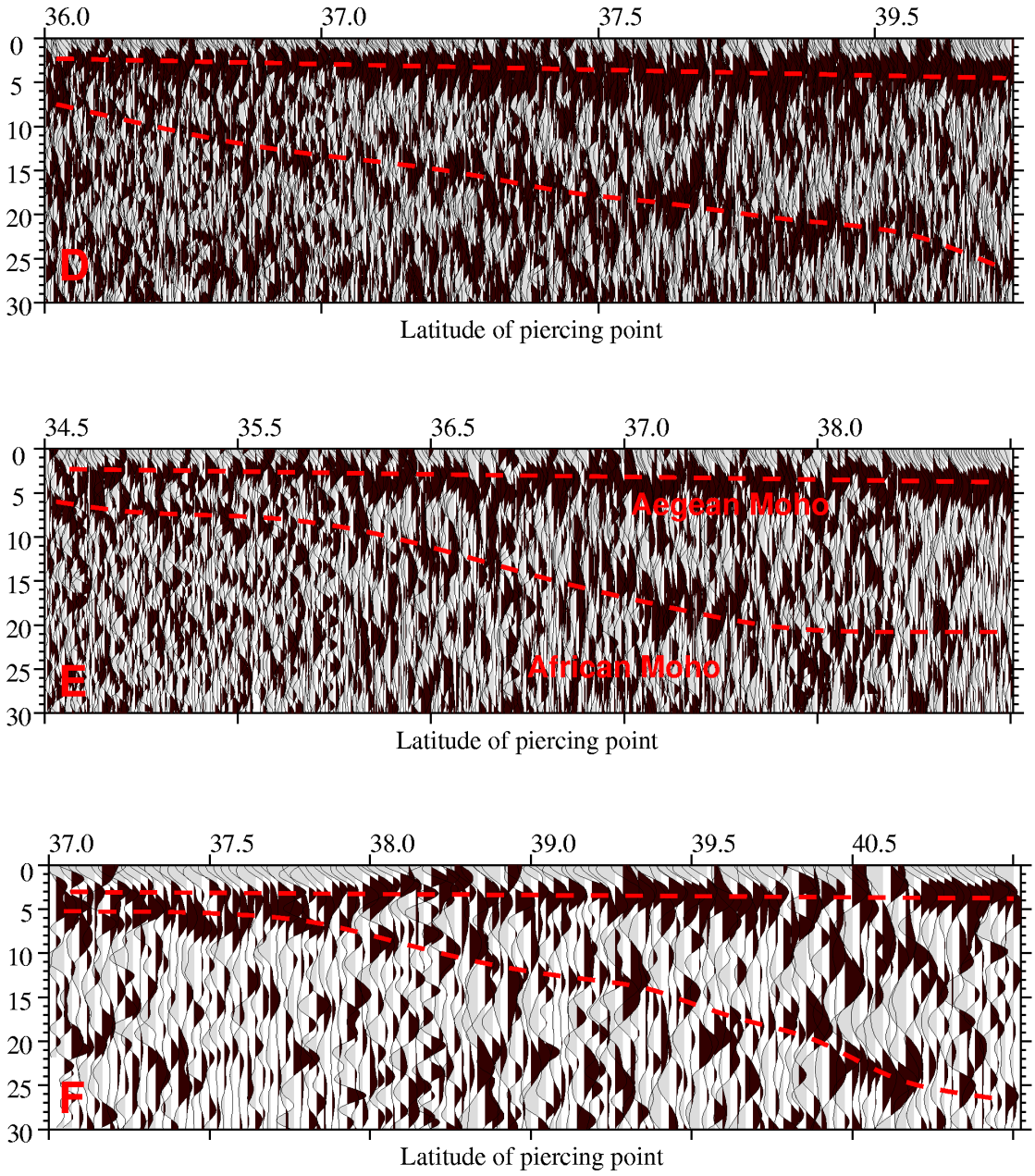

Fig. 5.15. Same as Figure 5.14 along profiles D-F located perpendicular to the trench. D) individual S receiver functions along profile D in the eastern part of the Hellenic arc. E) same for profile E in the middle part of the arc, which crosses the central Crete. F) same for profile F in the western part of the Hellenic arc. The slab is shallower imaged along profile F than along profiles D and E.

In profiles D-F, shown in Figure 5.15, the subducted slab is not as easily resolved as it is shown along profiles A-C. It is interesting to note although all three profiles begin from the Hellenic trench and include the forearc area, they demonstrate a significant Moho phase with positive amplitude in the forearc region, while P receiver functions exhibited a reversed Moho velocity contrast beneath stations located in the forearc.

Profile D located in the eastern part of the Hellenic arc indicates a steep subducted plate in this part in comparison with other parts of the arc. The continuity of the subducted plate up to northern Greece is well illustrated along this profile. This phase can be followed from 6 s beneath southeastern Aegean gradually down to 25 s under northwestern Greece.

Along profile E in the middle part of the Hellenic arc, the slab is identified at shallower depth (at about 5.5 s delay time) comparing with the eastern part of the arc. The dip of the subduction is low in the Cretan Sea and steepens significantly under the volcanic arc and reaches the delay time of about 20 s.

The slab is almost horizontal and is visible to about 24 s (220 km) beneath continental Greece. The slab depth along profile F is consistent with that from profile C in Figure 5.14. It shows a sub-horizontal slab beneath Peleponnesus at about 5 s and a sudden dipping in the northern Aegean Sea to a delay time of about 25 s. The main difference in slope of the slab can be also clearly seen along this profile.

5.2.6 Lithosphere-Asthenosphere boundary

The whole study area was divided into 39 non-overlapping boxes with respect to the distribution of Sp conversions at 80 km (Fig. 5.16). The size of each box corresponds roughly to the number of S receiver functions crossing that box. Since the Sp conversions are generally weak, a stacked S receiver function was computed for each box from many individual records. Prior to summation, the moveout correction for a reference slowness of 6.4 s/deg was applied. In Figure 5.17, the stacked S receiver functions computed in each box along profiles D-F (shown in Fig. 5.13) for piercing point at 80 km depth are plotted.

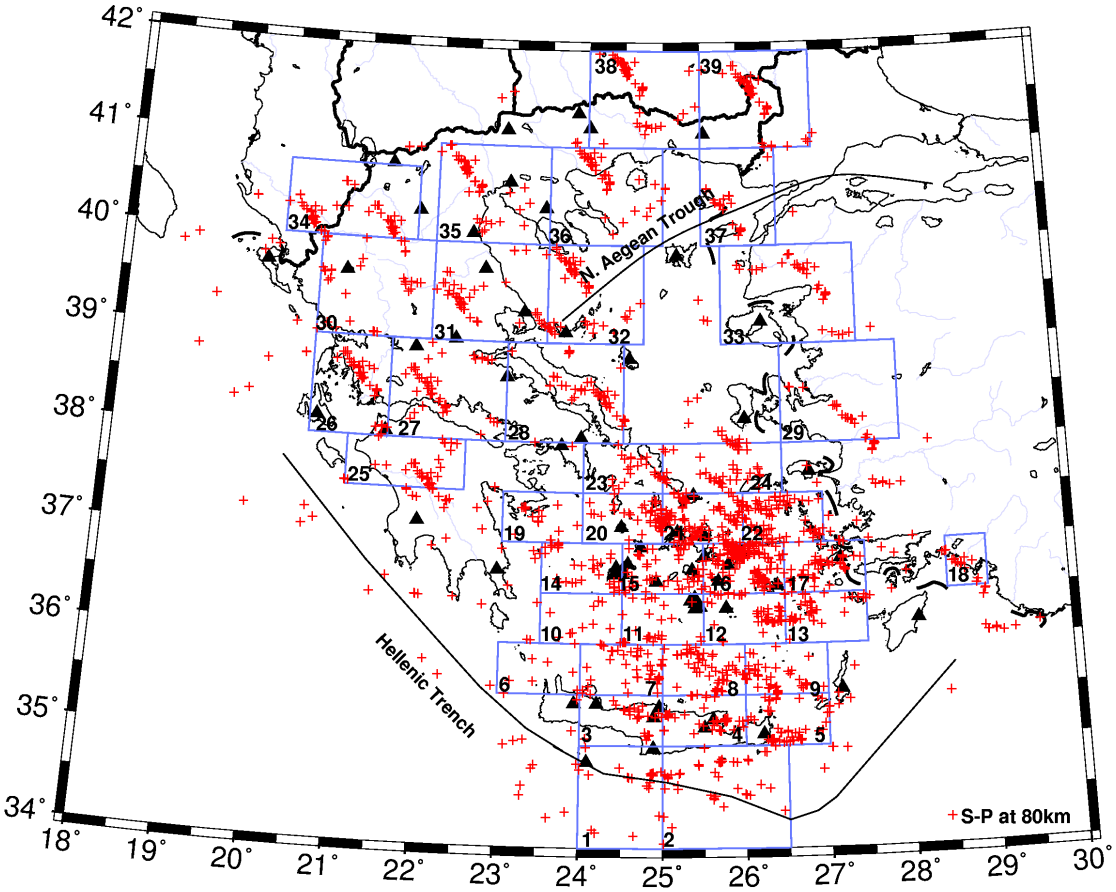

Fig. 5.16. The study area is divided into 39 non-overlapping boxes with respect to the Sp conversion points at 80 km. S receiver functions were computed for each box and a stacked S receiver function was obtained from many individual traces box by box.

Negative (positive) amplitudes, plotted in black (gray) indicate a velocity decrease (increase) with depth. A clear negative phase (labeled LAB) at ~ 12-25 s is apparent in sections D-E and is identified as a converted phase from the lithosphere-asthenosphere boundary. Figure 5.17 (D-F) show a consistent LAB phase beneath the Aegean to the continental Greece along different profiles. This phase is observed along profiles D and E located in the eastern and middle part of the Hellenic arc at a delay time of about 12 s under southern Crete, where it steepens significantly under the volcanic arc (Cyclades area) and arrives at about 25 s.

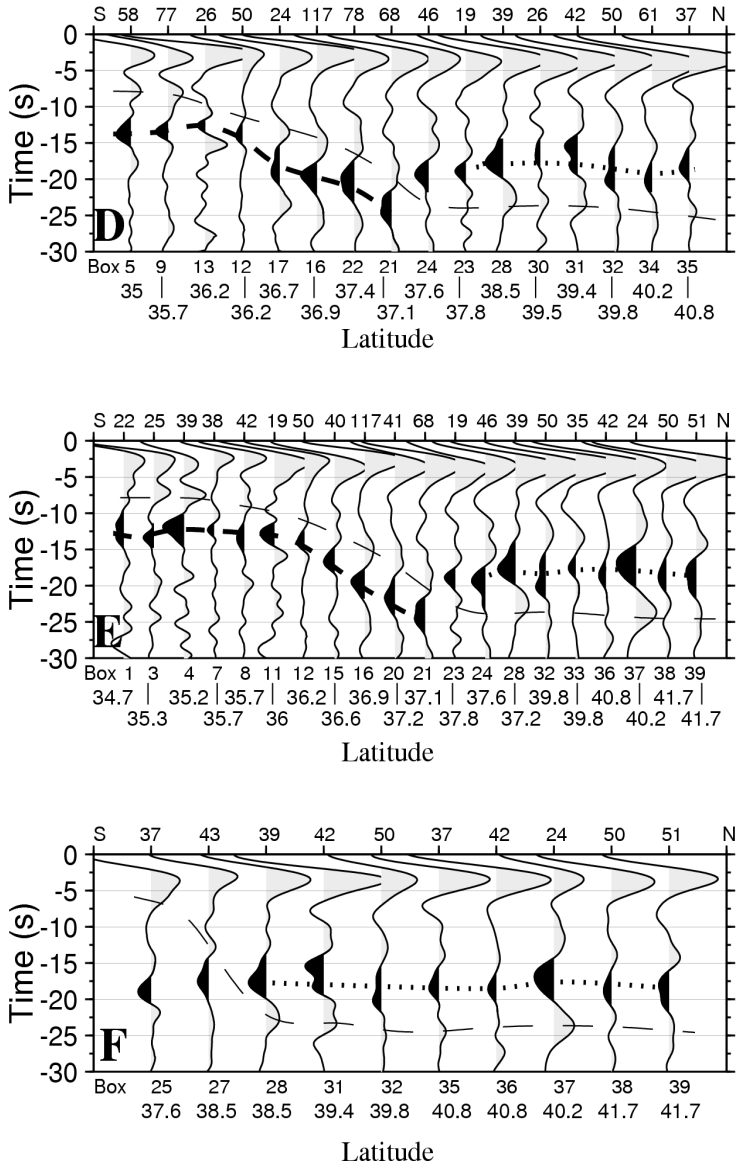

Fig. 5.17. Imaged lithosphere-asthenosphere boundary estimated by stacked S receiver functions, box by box, along profiles D-F (shown in Fig. 5.13). The box number and number of S receiver functions for each box are indicated in the lower and upper parts of the figures, respectively. The latitude of the center of the boxes are also shown below. Negative amplitudes of S receiver function (in black) show a velocity decreases with depth. Different types of dashed lines are used to demonstrate continental (dot-dashed) and oceanic (thick dashed) LAB. D) stacked S receiver functions, along profile D in eastern part of the trench, showing a clear negative phase dipping from 12-25 s beneath volcanic arc (box 21), which is interpreted as subducting African LAB. The continuity of LAB could not be imaged further north. Beneath northern Greece, LAB shallows to 17 s, interpreted as continental Aegean LAB. E) same along profile E in central part. F) same along profile F located in mainland Greece reliably shows the continental Aegean LAB at 17 s. The slab phase deduced from Fig. 5.14 & 5.15 is also shown with a thin dashed line, although it can not be well identified.

It shallows towards continental Greece and arrives at time of about 17 s. The observed slab phase deduced from Figures 5.14 & 5.15 can be also seen in the stacked S receiver functions, labeled with African Moho. Section F located in the western part of the arc, in mainland Greece reveals reliably another feature. A very strong negative phase at an almost constant time of 17 s can be significantly identified along this profile.

5.3 Discussions

In this part, the obtained results from P and S receiver functions are discussed and compared with the other current ideas in this region. They are also interpreted and finally three depth maps are presented for the crustal and upper mantle structure beneath the whole study area.

5.3.1 Thickness of the Lithosphere

The delay times of the LAB phase obtained from each box were converted into the depth by multiplication the arrival times of this phase with a factor of 9 using the IASP91 reference model. Figure 5.18 shows that in southern Crete as well as in the southern Aegean Sea the LAB is at about 100 km deep and dips down to 225 km towards central Aegean. Further north, beneath continental Greece, it thins to about 150 km. The average thickness of the lithosphere in the Mediterranean has been estimated to be 90 km (Papazachos, 1969; Payo, 1967,1969) for the Eurasian plate, although Calcagnile et al. (1982) showed that the lithosphere-asthenosphere boundary undulates between 90 and 120 km. The thickening of the LAB (from 100 to 225 km) towards the Aegean Sea can be interpreted as the subduction of the oceanic African lithosphere beneath the Aegean plate. Using S receiver functions, this boundary could be mapped up to the depth of 225 km.

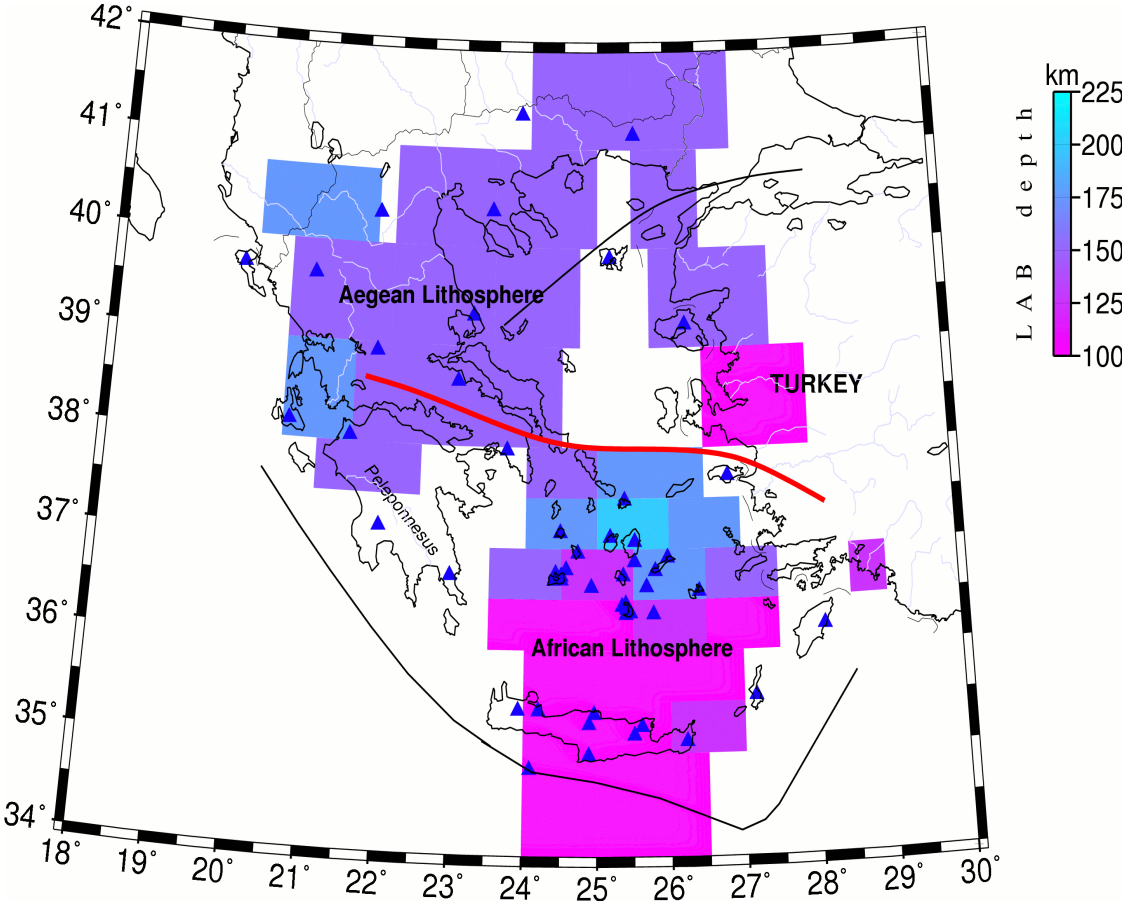

Fig. 5.18. The LAB depth map obtained from S receiver function analysis in Aegean. Time has been converted to depth using IASP91 reference model. The values are given in Table C.2, Appendix C. The heavy red line is a boundary separating the observed continental Aegean lithosphere from the oceanic African lithosphere.

The strong horizontal negative phase along profile F (Fig. 5.17), which is located at about 17 s above the slab phase in mainland Greece, is also interpreted as due to the continental Aegean lithosphere (Eurasian lithosphere), whose thickness is estimated to be about 150 km. It seems therefore that the African lithosphere is thinner than the Aegean (Eurasian) lithosphere at this place. This thicker lithosphere observed in the Aegean compared to Africa is surprising according to the large stretching (a factor of 2) accommodated since the Miocene (Le Pichon et al., 1982). However, most of the primary stretching affected the Sea of Crete where no information could be presented about the Aegean LAB. It may be also attributed to the crustal thickening across western and central Greece during the building process (Hellenides mountain range).

This difference in the LAB depth is therefore consistent with a localized stretching, affecting mostly the southern area of the Aegean, and different than the present day stretching evidenced in northern Aegean by GPS measurements.

5.3.2 Description of the Hellenic subduction zone

To calculate the slab depth from S receiver functions, an averaged delay time of the converted Sp phase due to the slab was determined from the stacked S receiver function obtained from each box and then transformed into a slab depth, using the IASP91 reference model. The delay times of the Sp conversions from the oceanic African Moho and computed slab depths are listed box by box in Table C.2, Appendix C. To construct a homogeneous slab depth map and image the geometry of the descending slab, slab depths obtained from both P and S receiver functions are used (Tables C.1 & C.2, Appendix C).

The results are demonstrated in Figure 5.19 and show the complex geometry of the subducted slab beneath the Aegean up to continental Greece. The depth of the slab is shallowest under western Peleponnesus, southern Crete and southeast of Rhodes and imaged at an average depth of about 40 km, it dips at various angles down into the Aegean Sea. It increases in depth to 160 km under the volcanic arc. Further north, beneath northern Greece, where no seismicity is related to this part of the slab, it is roughly horizontal at a depth of 220 km. Tomographic results (Spakman et al., 1988, 1993; Papazachos et al., 1995) show that the Benioff zone must extend as far north as the northern Greek border. The subducted slab obtained from tomography could be imaged down to 600km (Spakman et al., 1988) and even to 1200 km (Bijwaard et al., 1998) beneath northern Greece, even though the deepest earthquakes are located at depths of approximately 180 km in the eastern part of the trench. It seems therefore that the northern part of the slab is aseismic.

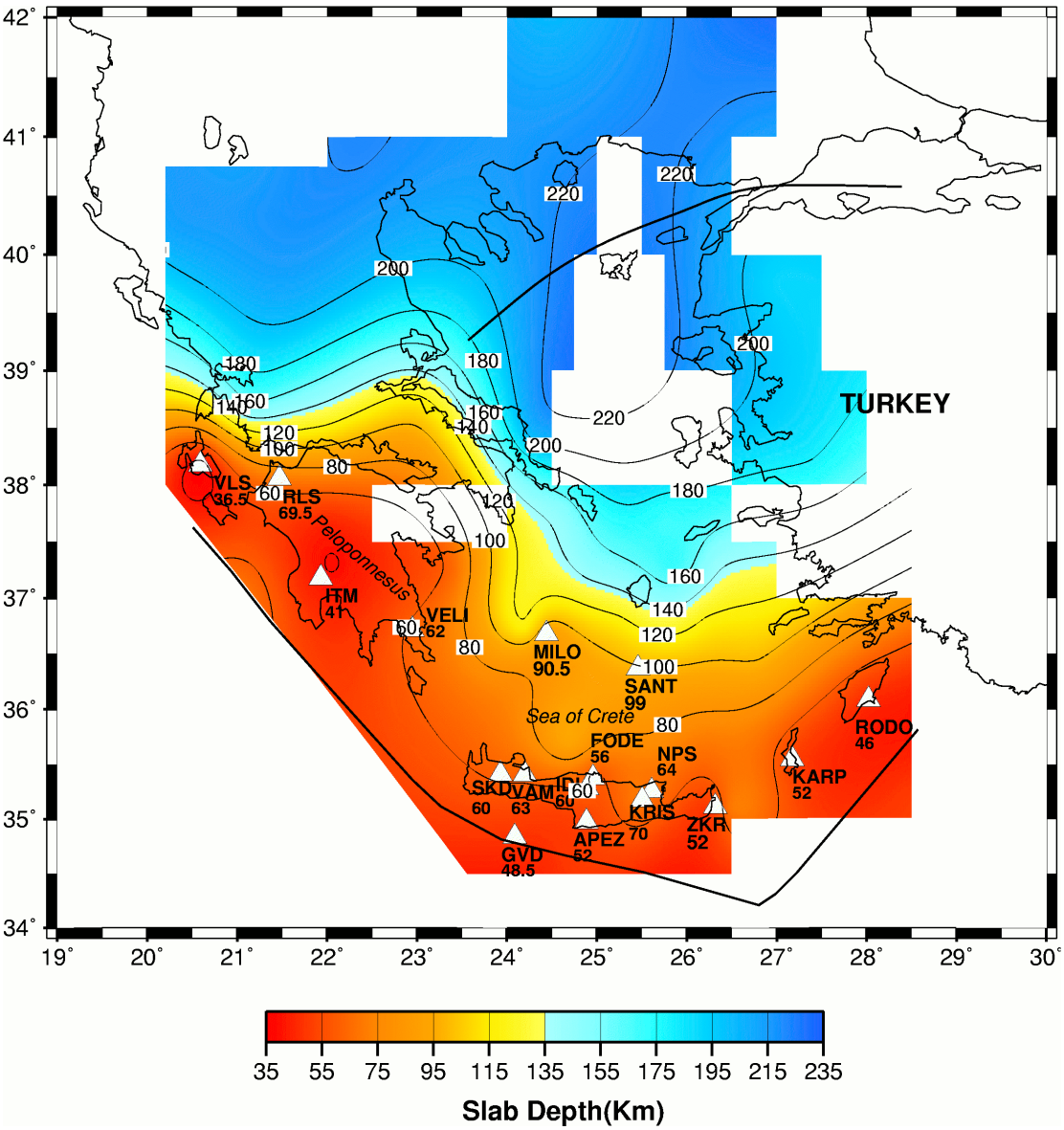

Fig. 5.19. Slab depth map obtained from both P snd S receiver functions. The slab depths for the stations (with clear Ps converted phase from slab) represented by triangles are computed using P receiver functions. The slab depths for the other parts of the area are obtained from the stacked S receiver functions, box by box. White boxes show the areas that not enough S piercing points are available.

It can also be argued that reheating of a downgoing slab can affect its rheological properties and limit, if not suppress seismicity (Wortel, 1982; Hatzfeld, 1994). Comparing the obtained results from this study with the results deduced from tomography may imply that receiver functions may only image the shallow dipping part of the slab down to 200 km.

Furthermore, the observed curvature of the slab seems to be less bent as we go deeper and northward suggesting that the subduction was more linear when it started. This supports the idea that subduction has migrated from the northern Aegean to its present position since Eocene (De Jonge et al., 1993).

The subducted slab is observed much deeper and also steeper in the eastern part in comparison with the western part of the arc, as Figure 5.19 shows. The slab is almost horizontal beneath the western part and observed at depth of ~ 50-60 km under Peleponnesus, it steepens strongly into the northern Aegean Sea and reaches a depth of approximately 200 km. This result is also consistent with the shallow seismicity recorded beneath the Peleponnesus (Hatzfeld et al., 1989; Papazachos et al., 2000).

The observed change in the slope of the slab is in good agreement with independent results in this area. Detailed tomographic results for this region (Papazachos & Nolet, 1997) confirm the change in dip within different parts of the subduction. Hatzfeld & Martin (1992), Hatzfeld et al, (1993), Papazachos et al. (2000) imaged the Wadati-Benioff zone in this area and showed that it dips at shallower angle in the west contrary to the eastern part. It seems also that the subduction occurs easierly in the eastern part, leading to a rapid sinking of the African plate beneath eastern part of the arc in accordance with GPS measurements, which showed a trenchward motion in the southeastern Aegean of 10 mm/yr relative to the whole southern Aegean (McClusky et al., 2000).

It is apparent from results of this study that there is no large tear in the slab resolved by S and P receiver functions. However, due to the lack of the seismological stations in the northern Aegean Sea, the continuity of the slab could not be imaged.

Regarding Figure 5.19, the slope of the slab varies laterally, as well as vertically northward. The lateral change in slope towards the eastern part of the subduction zone can be shown to be significant beneath the volcanic arc. A notable difference can be observed between the western and eastern part of the Cretan Sea, where the subducted slab is much deeper in the western part.

However, Spakman et al. (1988) found a continuous subducting slab along middle part of Hellenic arc, whereas they observed a tear at a depth of about 200 km beneath the

northern Aegean Sea and Greece. The observations of this study confirm the existence of a continuous slab beneath the middle part of the Hellenic arc and in contrast to Spakman et al. (1988) shows no tear in the downgoing slab beneath Greece and Peleponnesus.

The main difference in slope, interpreted as a kink at a depth of about 75-95 km along the western profile, reported by the tomographic images of Papazachos & Nolet (1997), can also be clearly seen by cross-sections C and F shown in Figures 5.14 & 5.15. This study confirms therefore the very shallow dipping slab (slope less than 10°), evidenced as far as northern Greece, that was mapped by Papazachos and Nolet (1997) and at shallower depth than proposed by Spakman et al. (1993).

5.3.3 Reversed continental Moho contrast complication

The derived S receiver function sections, as shown in Figures 5.14 & 5.15, present a clear normal Moho contrast (i.e. with positive amplitude) in the forearc area. To obtain a complete picture and look for the origin of the negative Ps converted phase in Crete, P and S receiver functions recorded in four stations are selected and compared; three of these stations are located in the forearc (SKD, IDI, NPS) and one of them in continental Greece (PLG). P and S receiver functions are then stacked and filtered using the same bandpass filter of 4-20 s. Figure 5.20 shows the computed P and S receiver functions for the four selected stations. However, only Ps and Sp conversions close to each station are selected in order to resolve the same structure beneath each area. Positive amplitudes are plotted in black. On both Ps and the Sp plots, the bold vector indicates the converted phase at the continental Moho, and the thin vector shows the converted phase from the subducted oceanic Moho for stations located along the Hellenic trench. As the Figure shows, no positive amplitude Moho conversions are seen on the P receiver function data at the three selected stations located at the forearc. Instead, strong converted phases with notable negative amplitudes appear at delay times of 3-4 s (marked with bold vector).

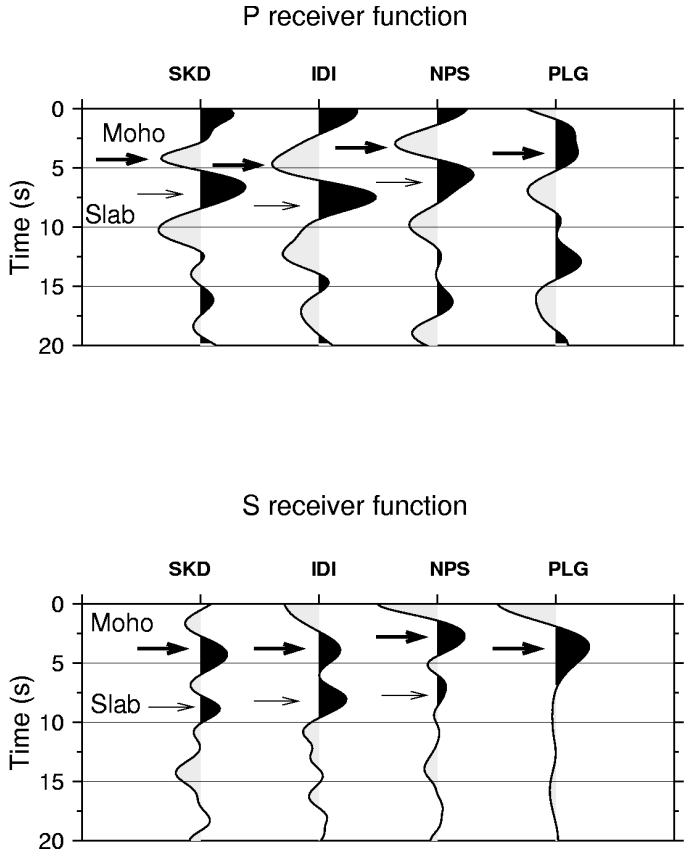

Fig. 5.20. Comparison of P and S receiver functions for four selected stations in order to check their compatibility. Stacked P receiver functions in upper panel show notable negative conversions, indicated with bold arrows at expected Moho times for stations located in the forearc (SKD, IDI, NPS), while this conversion is positive for station PLG in mainland Greece. The interpreted slab phase is indicated with thin arrows. Stacked S receiver functions in lower panel show clear positive conversions at expected Moho times for all four stations. Both type of receiver functions show positive amplitudes for the slab phase. The small difference in arrival times of the slab phase is due to the different locations of the P and S piercing points.

This negative amplitude for P receiver functions recorded in Crete has been a subject of debate. Knapmeyer et al. (2000) interpreted the weak negative signal recorded in western Crete as due to a thick fossil accretionary wedge. Li et al. (2003) interpreted the negative phase recorded in western and northern central Crete as due to a reversed Moho velocity contrast caused by a large amount of serpentinite in the mantle wedge.

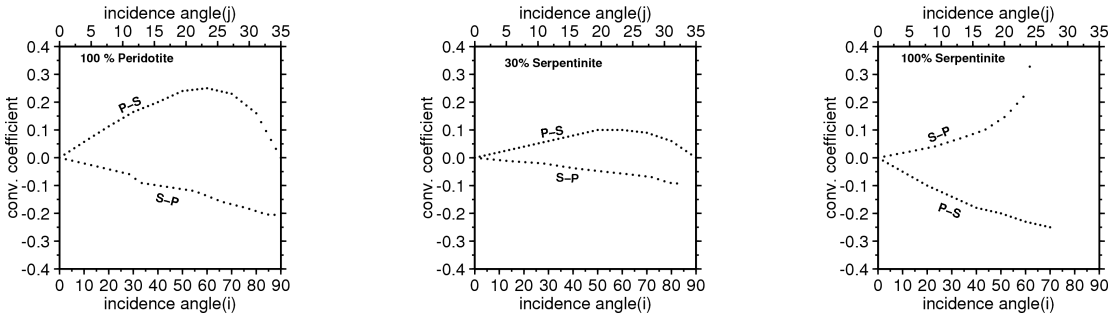

(a) (b) (c)

Fig. 5.21. Calculated Ps and Sp conversion coefficients for different uppermost mantles. a) those for a normal crust overlain by 100% peridotite uppermost mantle. b) if the uppermost mantle consists of 30% serpentinite. c) for a completely serpentinized uppermost mantle, note that the values are reversed and Ps conversion coefficients are no longer positive.

Finally, Endrun et al. (2004) concluded that beneath western Crete a thick crust extends down to the oceanic lithosphere.

Using the combination of both P and S receiver functions results in discrimination between different models. The stacked S receiver functions obtained from three stations at the forearc reveal, contrary to the computed P receiver functions, the presence of a normal Moho contrast beneath these stations. Furthermore, although the Moho converted phases reveal different polarities for P and S receiver functions for stations located at the forearc, they have the same polarity for the station located on mainland Greece and arrive at the same time. We consider three different crust-mantle contrasts (Hacker, 2003) and calculate their corresponding Ps and Sp conversion coefficients (Fig. 16). A normal crust overlain by 100% peridotite uppermost mantle shows a positive Ps and a negative Sp conversion coefficient. If the uppermost mantle contains 30% serpentinite, Ps conversion coefficients tend to have smaller values, while those of Sp increase. It is interesting to note that for a completely serpentinized uppermost mantle the values are reversed, Ps conversion coefficients become negative and those of Sp are positive. Therefore, a large amonut of serpentinite (larger than 30%) can provide a negative Ps conversion coefficient leading to a negative amplitude Ps conversions in the forearc.

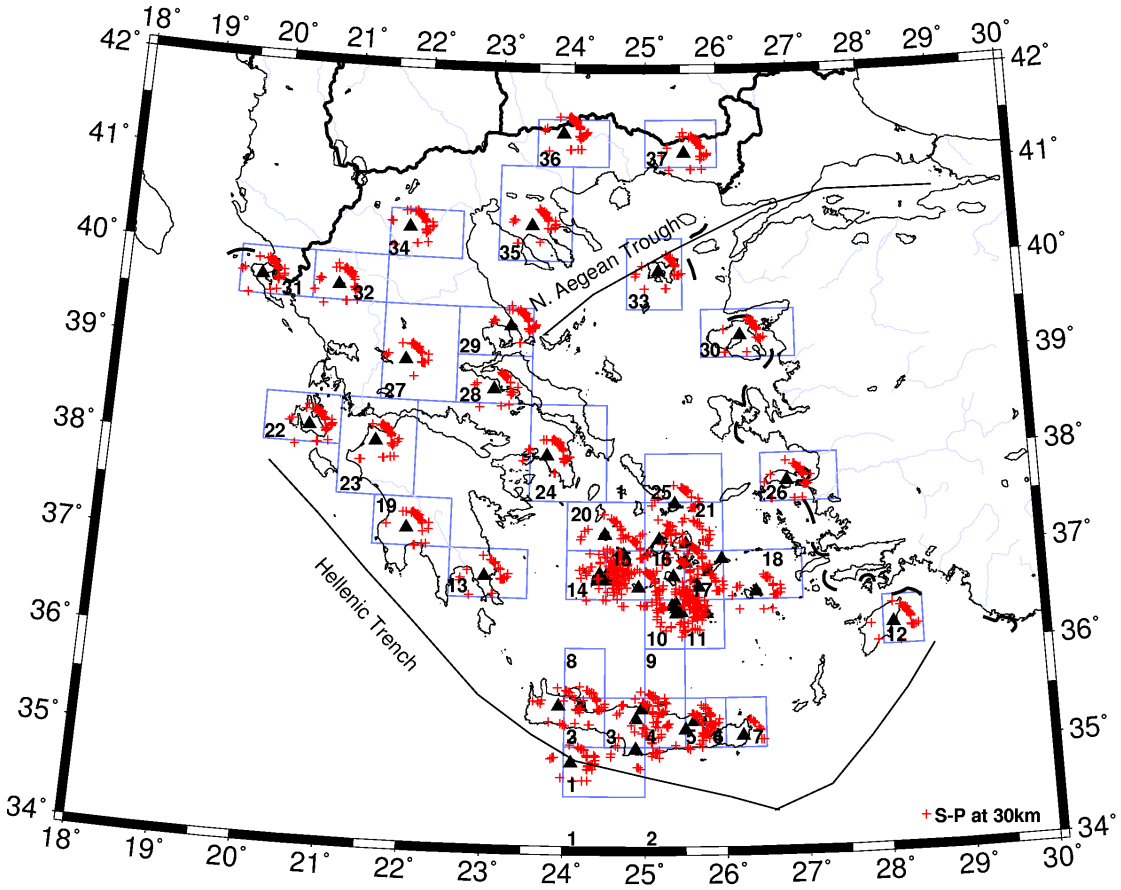

Fig. 5.22 The study area is divided into 37 boxes with respect to the Sp conversion points at 30 km. S receiver functions were calculated for each box and a stacked S receiver function was obtained from many individual traces box by box. The delay times of Sp conversions from Moho were converted into depth using IASP91 reference model.

It may concluded from these calculations that 50-60% serpentinization in the forearc could result in a negative contrast for P-to-S conversion, even though the Sp conversion coefficient remains negative.

5.3.4 Crustal thickness of the Aegean plate

Moho depth values obtained from P receiver functions (Table C.1, Appendix C) are complimented by using the stacked S receiver functions in each box shown in Figure 5.22 Figure 5.22 shows the distribution of Sp piercing points at 30 km (average depth of the Moho).

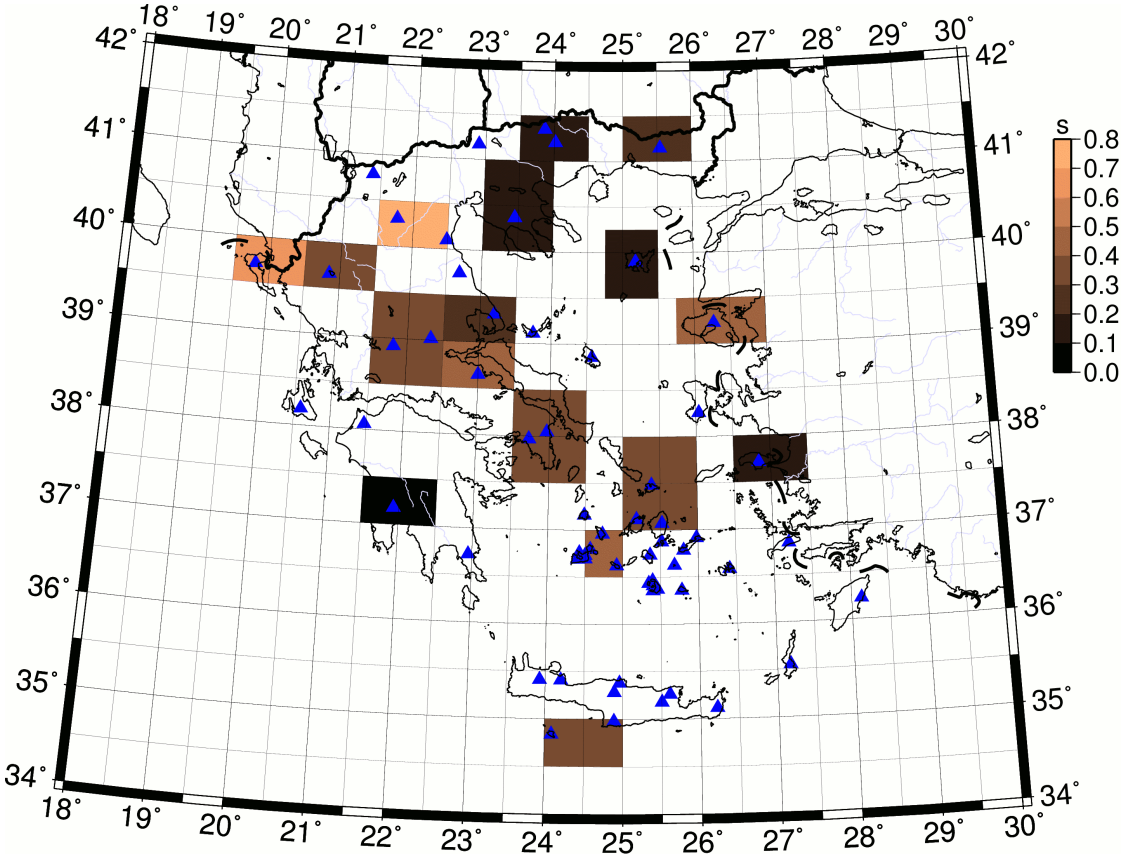

Fig. 5.23. Estimated time differences of the positive conversions at Moho obtained from P and S receiver functions. The maximum difference (0.7 s or ~ 6 km) is observed for western coast of Greece.

By combining both the P and S receiver function results, a more detailed, homogeneous map of the Moho depth for the whole Aegean area can be proposed.

The Moho depth is evaluated by converting the delay times of the Sp Moho phases into depth using a crustal Vp velocity of 6.2 km/s and Vp/Vs ratio of 1.73. These values are also listed in Table C.3, Appendix C. To propose a Moho depth map two factors need to be considered. First, it has to be checked that the Moho depths calculated from P receiver functions beneath each station agree with the depths computed from stacked S receiver functions for each box encompassing the station. This goal was achieved by calculating the time difference between the estimated Ps and Sp converted phases from the Moho boundary. Figure 5.23 shows the calculated time differences for the areas where a normal Moho contrast was seen using both methods.

Regarding Figure 5.23, the time differences are small and vary between 0-0.7 s (i.e. less than ~ 6 km in depth) and usually less than 0.4 s (~ 3 km), which is within our uncertainties. Second, a homogeneous map using both P and S receiver functions are built. For all stations in the back arc area, the Moho depths calculated by P receiver functions are used, because they are clear and more precise. For stations in the forearc region, where no positive Ps converted Moho phase could be determined, S receiver functions were utilized. Furthermore, due to the wider lateral distribution of piercing points for the S receiver functions compared to those of P receiver functions as well as the overlap of S piercing points from neighbor stations in some areas, a better coverage between stations is achieved.

All Moho depth estimates obtained from both P and S receiver functions (Tables C.1 & C.3, Appendix C) are used to generate a Moho map. The results are also complemented using Moho depths from 3 stations in Turkey (Saunders et al., 1998). However, to present a Moho depth map, the P receiver function results of some stations needs to be discussed as follows.

5.3.4.1 The observed Moho phase beneath PENT and ATH

Figure 5.24 shows the computed P receiver functions for two neighbor stations, PENT and ATH located in mainland Greece. Considering arrival times of the converted Ps phase from the Moho, the observed difference seems to be large for neighbor stations (3.1 s for ATH and 4.5 s for PENT). However, the computed stacked S receiver function obtained from box 24 includes this area (Fig. 5.22) and shows a Moho depth of about 28 km. This value is in good agreement with the computed Moho depth from P receiver functions for station ATH (~ 26 km). Due to the sparse data recorded at station PENT (24) and to the large difference in the computed Moho depth relative to its neighbor station ATH, the depth estimate from this station is not used in the Moho map, because it seems unrealistic to have such large offset in the Moho considering the gravity map.

5.3.4.2 Presence of thick Moho under SANT

For the stations MILO and SANT, located on the volcanic islands in the Cyclades region, two similar phases at about 2.5 and 4.5 s (i.e. ~ 20 and 36 km) are seen in the P receiver functions. Both of these phases arrive within the expected Moho delay time and appear to be stable and coherent (Fig. 5.25). The obtained S receiver functions from the corresponding boxes including SANT and MILO (boxes 10 and 15) seem different. The computed Moho depth from box 15 shows a Moho depth of 33 km (at ~ 4 s), while box 10 reveals a Moho at the depth of approximately 25 km (~ 3 s). As Figure 5.22 shows the distribution of the Sp piercing points in box 10 can not well cover the station SANT. Therefore the second phase in the P receiver functions is interpreted as the converted Moho phase, it shows however a larger amplitude than phase 1 at station SANT. It is suspected that phase 1 is produced by multiple scattering from sediment and upper crustal layers, that are usually present under

volcanic islands.

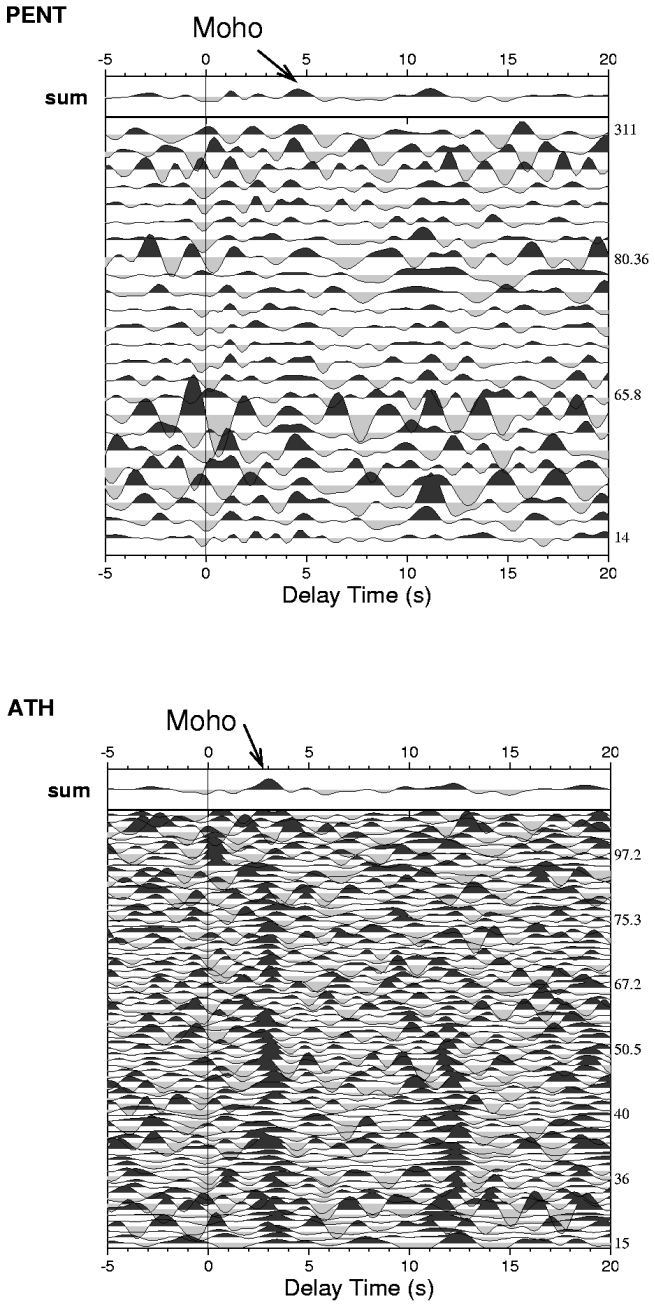

Fig. 5.24. Individual P receiver functions sorted after back azimuth (shown in the right) for two neighbor stations PENT and ATH in mainland Greece. The Ps converted phases from Moho observed at 4.5 and 3.1 s, respectively. This difference seems to be large. Although PENT shows sparse data compared to ATH.

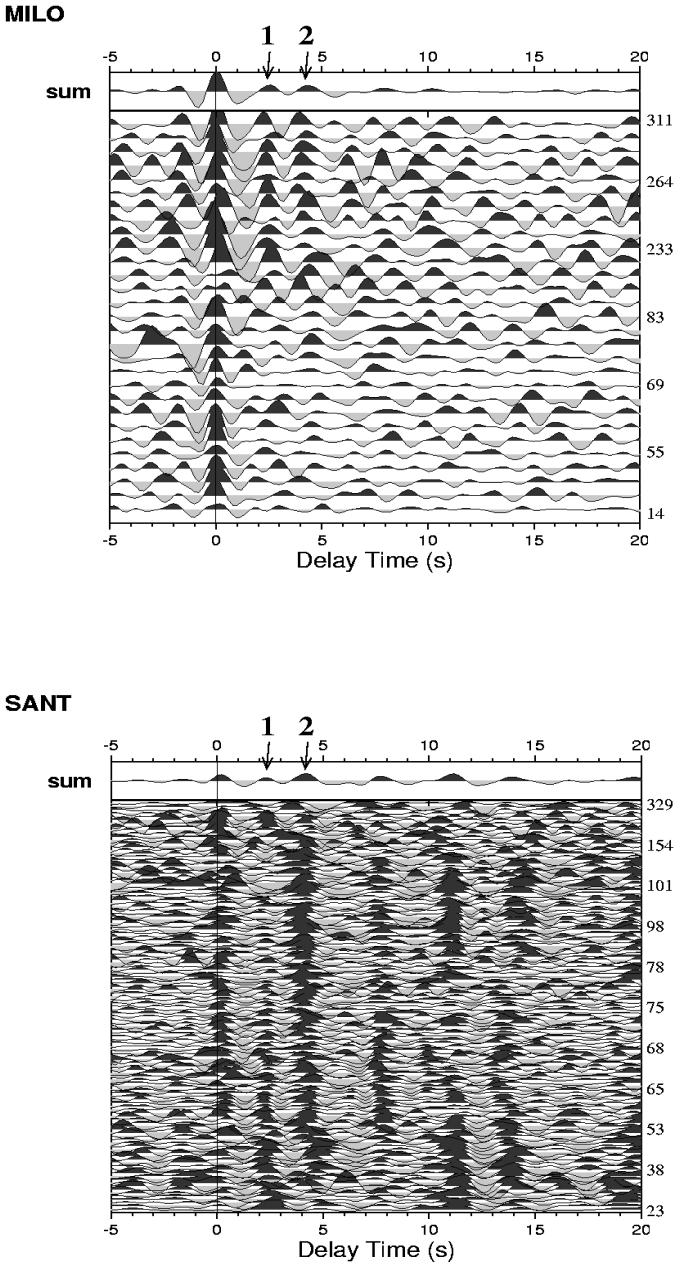

Fig. 5.25. Individual P receiver functions for two stations located on the volcanic islands of Cyclades region are sorted after back azimuth. Receiver function data show two coherent phases between 2-4 s labeled with 1 and 2, respectively. Regarding multiple scattering obtained from sediment and upper crustal layers presented in volcanic regions, phase 2 in interpreted as due to the Moho.

Li et al. (2003) observed significant energy on the transverse component at station SANT, which correlates well with the converted Moho phase at 4.2 s on the radial component. They interpreted this observation as due to an anisotropic crustal structure. They also showed that the boundary at 25 km depth may be related to the Moho of the Aegean subplate which overlies a thinned remnant of the Cretan microcontinent whose lower boundary (Moho) is located at 34 km.

5.3.4.3 Moho depth map

A map of the Moho depth that summarizes the results of this study is presented in Figure 5.26. A crust of approximately 32-38 km is observed beneath western Greece along the Hellenides mountain range. The correlation of thick crust and the remarkably high elevation beneath western Greece indicates an isostatic crustal balance, implying a distributed crustal thickening as the main mechanism of the crustal thickening in this area. This estimation of the crustal thickness is however less than previous studies for this region, where depths were indicated to be ~ 40-46 km (Makris, 1976; Ligdas & Lees, 1993; Papazachos, 1998; Tiberi et al., 2000; Karagianni et al., 2002, 2005).

Moving toward the west coast of the Aegean Sea, the crust thins to the depth of 28-30 km consistent with the result of Makris (1978) beneath Evia. This thin crust is likely to be due to the extension tectonics that affected the whole Aegean and adjacent areas. The crustal thickness under the Peleponnesus is estimated to be about 25-28 km, since the first phase at 3-3.5 s (shown in Fig. 5.14(C), 5.15(F)) as the converted phase from the Moho discontinuity is reliably assumed. Rather than a Moho at a depth of 45 km as suggested by other authors (Karagianni et al., 2002; van der Meijde et al., 2003; Karagianni et al, 2005), it is suggested by this study that the second phase at about 4.5-5 s delay time defines the oceanic Moho of the subducting plate beneath the Peleponnesus as also suggested by the seismicity reported for this area.

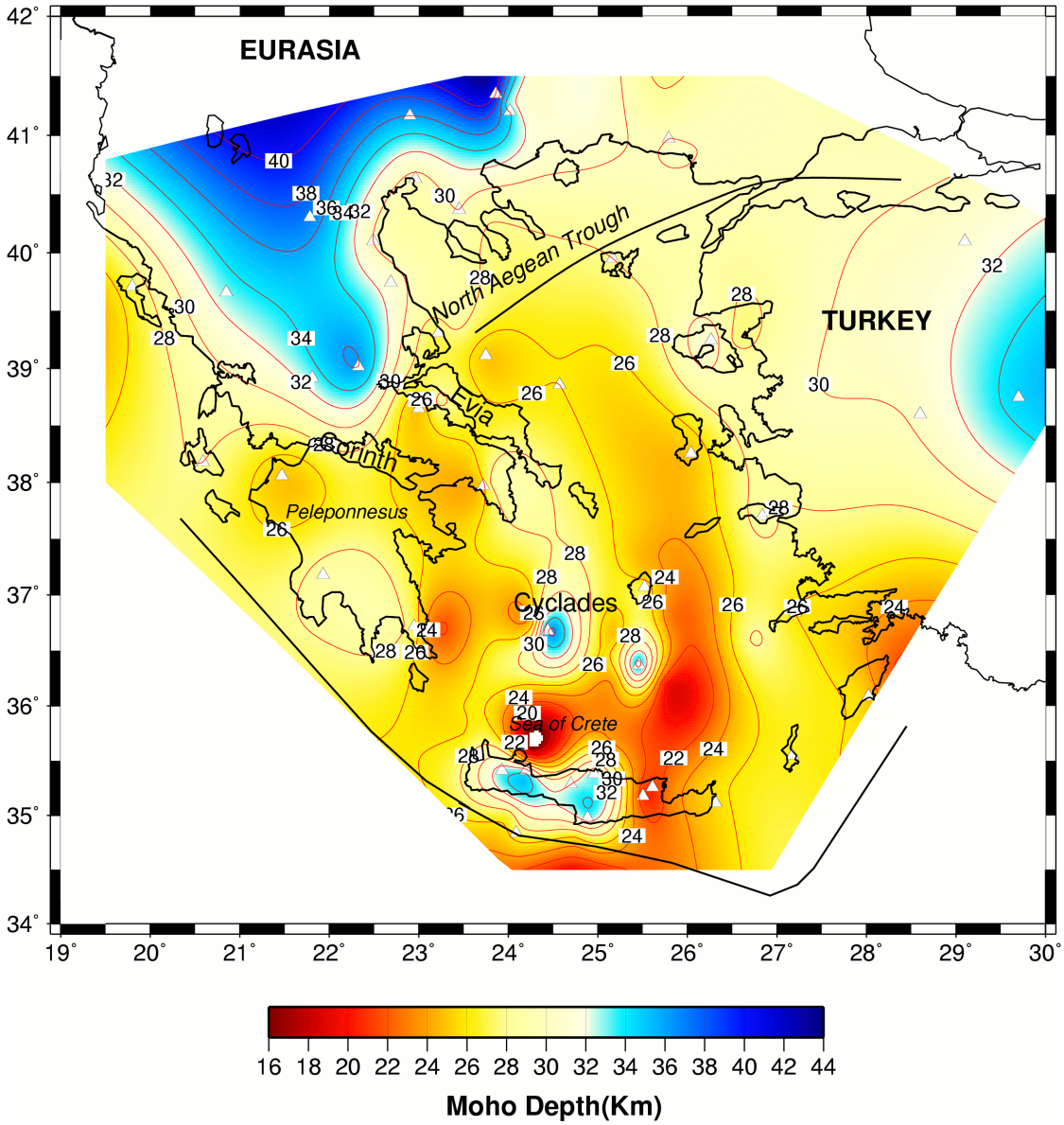

Fig. 5.26. The Moho depth map (in km) deduced from P and S receiver functions. The Moho depth values of three stations are from Saundres et al. 1998. The Moho depths used for this map are listed in Tables C.1 & C.3, Appendix C.

The resulted Moho depth estimates a crustal thickness of 25-29 km beneath Evia and Corinth Gulf, north of Peleponnesus, which are consistent with the Moho depths derived from inversion of gravity anomaly data by Tiberi et al. (2001). In the northern Aegean, a region that has undergone crustal extension since the Eocene, a thin crust of approximately 25-28 km is imaged.

Travel time (Papazachos, 1998) and shear wave velocity (Karagianni et al., 2005) tomographies also show a thin crust in this area. Wide angle reflection profiles, conducted in the Sporades Basin(near station SKOP) show a Moho depth at about 25 km (Vigner, 2002).

Beneath the southern Aegean Basin, a very thin crust of about 20-22 km is observed, which reaches 26 km eastwards. These results are also in good agreement with Moho depths obtained from seismic profiles (Makris, 1978; Bohnhoff et al., 2001), shear wave velocity tomography (Karagianni et al., 2005) and receiver function analysis (van der Meijde et al., 2003) for this region. Such a thickness would indicate significant thinning of the crust within this area in comparison to the northern Aegean area. The absence of large thinning associated with the North Aegean Trough, that is a region with the highest present day strain rate computed by GPS measurements, confirms a recent evolution in the geodynamics of the North Aegean Trough suggested by Armijo et al. (1996).

A thicker crust is observed beneath the central Aegean across the Cyclades region. The Moho depth in this part is estimated to be about 25-30 km. Refraction data (Makris, 1978, Vigner, 2002) indicated a Moho depth of about 28 km in this region. These values may confirm the idea that the Cyclades act such a rigid block which do not stretch during the second episode of the extension (which affects significantly the northern Aegean Sea). However, the crustal thickness displays a sudden thickening beneath stations MILO and SANT on the volcanic islands and reaches depths to 36 and 34 km, respectively. This value has been already suggested by Li et al. (2003) beneath station SANT, and is consistent with results derived from gravity studies in this region (Tirel et al., 2005).

A large difference in Moho depths has been reported beneath the island of Crete (Bohnhoff et al., 2001; Li et al., 2003). Makris (1978) showed an average depth of about 30-32 km beneath Crete, whereas Bohnhoff et al. (2001) revealed a crustal thickness of approximately 32 km in the central Crete which thins to 24 and 26 km eastwards and westwards, respectively. Li et al. (2003) showed that crustal thickness varies between 31-39 beneath the island of Crete. The observations of this study are

concluded that the crustal thickness beneath western and central Crete is estimated to be about 30-33 km and thins to 21-25 km under the eastern part of this island.

Based on this study, the stretching scenario in the Aegean will be modified in the way that a thinner crust is inferred as the unstretched crust in mainland Greece (32-38 km) and therefore suggested a stretching factor of 20-25% in the northern Aegean and 40-45% in the Cretan Sea. It seems also, contrary to the previous works, that a low to moderate extension has occurred in the whole region (Makris, 1978; Angelier et al., 1982). The resulted Moho map fits well in the sea with the inferred gravity map (Tsokas & Hansen, 1997; Tirel et al, 2005), however it is smoother than what is expected from tectonics. The Moho estimations reliably show that the continental crust along Hellenides mountains beneath Peleponnesus and Crete were also affected by the extension occurred in the Aegean, consistent with the GPS results in the southern Aegean (McClusky et al., 2000).

However, not similar reactions of the different parts of Crete to the extension resulted in a thicker crust in its western block. No NE-SW trend associated with the North Aegean Trough as inferred by gravity (Tirel et al., 2005) is observed by this study and may indicate that the North Aegean Trough is only a superficial feature not affect really the crustal thickness beneath this area. Finally, the relatively smooth Moho topography in the northern Aegean Sea (excluding MILO and SANT, whose thicknesses are related to the volcanic structure) is suggested from this study that varies between 25-29 km. This favors a “ductile” tectonic type for the extension instead of a chaotic horst and graben extension type.